Free vibrations of FG elastic Timoshenko nano-beams by strain gradient and stress-driven nonlocal models

R. Barretta[a,*], S. Ali Faghidian[b], R. Luciano[c], C.M. Medaglia[d], R. Penna[e]

[a] Department of Structures for Engineering and Architecture, University of Naples Federico II, via Claudio 21, 80125, Naples, Italy
[b] Department of Mechanical Engineering, Science and Research Branch, Islamic Azad University, Tehran, Iran
[c] Department of Civil and Mechanical Engineering, University of Cassino and Southern Lazio, via G. Di Biasio 43, 03043, Cassino, FR, Italy
[d] Link Campus University, via del Casale di San Pio V 44, 00165, Rome, Italy
[e] Department of Civil Engineering, University of Salerno, via Giovanni Paolo II, 132 - 84084, Fisciano, Sa, Italy

ABSTRACT

Size-dependent vibrational behavior of functionally graded (FG) Timoshenko nano-beams is investigated by strain gradient and stress-driven nonlocal integral theories of elasticity. Hellinger-Reissner's variational principle is preliminarily exploited to establish the equations governing the elastodynamic problem of FG strain gradient Timoshenko nano-beams. Differential and boundary conditions of dynamical equilibrium of FG Timoshenko nano-beams, with nonlocal behavior described by the stress-driven integral theory, are formulated. Free vibrational responses of simple structures of technical interest, associated with nonlocal stress-driven and strain gradient strategies, are analytically evaluated and compared in detail. The stress-driven nonlocal model for FG Timoshenko nano-beams provides an effective tool for dynamical analyses of stubby composite parts of Nano-Electro-Mechanical Systems.

1. Introduction

Numerous researches have been carried out in recent years on size-dependent mechanical models which are capable of capturing small scale effects exhibited by nanostructures [1,2]. Scale phenomena are described by introducing characteristic lengths in constitutive relations. In the framework of gradient elasticity theory, the material response at a point of a continuous structure depends not only on the classical material fields, but also on their gradients [3]. Several size-dependent models have been recently proposed in literature, such as unified gradient elasticity [4–7], enhanced nonlocal formulation [8] and homogenization theories [9–14]. Based on Mindlin's strain gradient elasticity [15], valuable contributions were provided by Aifantis in Ref. [16] and advanced to second-order strain gradient materials by Polizzotto [17]. The classical (strain-driven) nonlocal theory of elasticity was proposed by Eringen [18,19], in which the stress field is the integral convolution between elastic deformation field and a positive-decaying averaging kernel. For unbounded structural domains, Eringen's integral law, equipped with Helmholtz's averaging kernel, can be considered equivalent to a suitable differential equation, due to tacit fulfillment of vanishing boundary conditions at infinity [20]. Equivalence does not hold for bounded domains, since suitable higher-order homogeneous constitutive boundary conditions have to be prescribed. Accordingly, for bounded nanostructures, Eringen's strain-driven integral convolution cannot be replaced with a differential constitutive equation [21,22]. As illustrated in Ref. [23], the strain-driven purely nonlocal elastic problems defined on bounded domains are ill-posed due to incompatibility between the higher-order constitutive boundary conditions and equilibrium requirements. These difficulties can be overcome by adopting the stress-driven nonlocal integral theory, recently introduced by G. Romano and R. Barretta [24]. This new methodology has been successfully applied to investigate flexural [25–27] and torsional static behaviors [28,29] and transverse and longitudinal free vibrations [30–32] of Bernoulli-Euler elastic nano-beams.

The motivation of the present study is in investigating size-dependent free vibrations of Timoshenko FG nano-beams by using the stress-driven nonlocal integral theory of elasticity. The plan is the following. Essential relations concerning FG linearly elastic materials are preliminarily collected in Sect.2. The elastodynamic problems of Timoshenko FG nano-beams, with strain gradient and nonlocal stress-driven elastic behaviors, are formulated in Sect.3 and Sect.4 respectively. An effective analytical solution procedure is illustrated in Sect.5

* Corresponding author.
E-mail addresses: rabarret@unina.it (R. Barretta), faghidian@gmail.com (S.A. Faghidian), luciano@unicas.it (R. Luciano), c.medaglia@unilink.it (C.M. Medaglia), rpenna@unisa.it (R. Penna).

The final version ofthis manuscript is available in COMPOSITES. PART B, ENGINEERING. DOI: 10.1016/j.compositesb.2018.07.036

to assess size-dependent dynamical response of FG Timoshenko elastic nano-beams. The main outcomes of the present paper are summarized in Sect.6.

2. Functionally graded materials

A functionally graded (FG) straight nano-beam of length L, with rectangular cross section Ω of width b and height h is considered. Cross-sectional principal axes of geometric inertia originating at the geometric centre O are denoted by $\bar{y}$ and $\bar{z}$, as depicted in Fig. 1.

The FG nano-beam is assumed to be made of two different elastically homogeneous materials with material densities ρ_1, ρ_2, Euler-Young moduli E_1, E_2, Poisson ratio $\nu_1 = \nu_2 = \nu$ and shear moduli $G_1 = E_1/2(1+\nu)$ and $G_2 = E_2/2(1+\nu)$. Effective material properties of the FG nano-beam, continuously varying across the bending direction (thickness) $\bar{z}$, are described by density $\rho(\bar{z})$, Euler-Young modulus $E(\bar{z})$ and shear modulus $G(\bar{z}) = E(\bar{z})/2(1+\nu)$ according to the rule of mixtures. Accordingly, density $\rho(\bar{z})$ and Euler-Young modulus $E(\bar{z})$ are assumed to vary along the thickness according to the power-laws [33].

$$E(\bar{z}) = E_1 + (E_2 - E_1)\left(\frac{1}{2} + \frac{\bar{z}}{h}\right)^n$$
$$\rho(\bar{z}) = \rho_1 + (\rho_2 - \rho_1)\left(\frac{1}{2} + \frac{\bar{z}}{h}\right)^n \tag{1}$$

where the subscripts 1 and 2 designate constituents 1and 2. The power-law exponent n is the non-negative parameter describing the material variation through the nano-beam thickness.

It is known that for FG cross-sections, the position of the elastic centre C, where the neutral axis passes through it, depends on the material distribution of Euler-Young moduli. Due to varying the effective material properties, the elastic centre does not coincide with the geometric centre, but it is shifted from the geometric centre as

$$\bar{z}_C = \frac{\iint_\Omega E(\bar{z})\bar{z}\,dA}{\iint_\Omega E(\bar{z})\,dA} \tag{2}$$

Accordingly, in the new Cartesian reference system at C, $z = \bar{z} - \bar{z}_C$ and $y = \bar{y}$. For FG rectangular cross-sections, the position of the elastic centre C is given by Ref. [34].

$$\bar{z}_C = \frac{n(E_2 - E_1)}{2(2+n)(E_2 + nE_1)}h \tag{3}$$

Furthermore, determination of the bending stiffness and shear area of FG Timoshenko nano-beams is useful in subsequent relations. Bending stiffness I_E is defined by the second moment of elastic area, weighted with the scalar field of Euler-Young moduli, about the y axis and is evaluated considering the bending abscissa $z = \bar{z} - \bar{z}_C$ originating at the elastic centre C. Similarly, the shear area A_G is defined by the elastic cross-sectional area weighted with the scalar field of shear moduli

$$I_E = \iint_\Omega E(z)z^2 dA, \qquad A_G = \iint_\Omega G(z)dA \tag{4}$$

Utilizing the effective Euler-Young modulus $E(z)$ and shear modulus $G(z)$ introduced above, bending stiffness and shear area are given by Ref. [34].

$$I_E = \frac{12E_2^2 + n(7+n(4+n))(4E_1E_2 + nE_1^2)}{(2+n)^2(3+n)(E_2+nE_1)}I_{\bar{y}}$$
$$A_G = \frac{G_2 + nG_1}{1+n}A \tag{5}$$

where $I_{\bar{y}} = bh^3/12$ is the second geometric moment of area of the cross-section about the $\bar{y}$-axis about the geometric centre and $A = bh$ is the cross-sectional area. Similarly, effective cross-sectional mass A_ρ and rotatory inertia I_ρ can be determined employing the previously introduced effective material density $\rho(z)$

$$I_\rho = \iint_\Omega \rho(z)z^2 dA = \frac{12\rho_2^2 + n(7+n(4+n))(4\rho_1\rho_2 + n\rho_1^2)}{(2+n)^2(3+n)(\rho_2+n\rho_1)}I_{\bar{y}}$$
$$A_\rho = \iint_\Omega \rho(z)dA = \frac{\rho_2 + n\rho_1}{1+n}A \tag{6}$$

It is inferred from Eqs. (5) and (6) that as $n \to 0$ and $n \to \infty$, the aforementioned material quantities approach the corresponding material quantities of constituent 2 and 1, respectively. A detailed analysis of elastic properties of FG rectangular cross-sections is provided in Ref. [34]. Recent papers on mechanics of FG Bernoulli-Euler, Timoshenko and higher-order shear deformable nano-beams can be found in Refs. [35–45] [46–51], and [52,53] respectively.

3. Strain gradient theory of elasticity for FG Timoshenko nanobeams

The elastodynamic problem of a FG Timoshenko nano-beam in the framework of the strain gradient theory of elasticity is formulated by making recourse to Hellinger–Reissner's variational principle [54]. The triplet (x, y, z) of axes is chosen along the length, thickness and width of the nano-beam, originating at the elastic centre. The plane of flexure is described by the pair x–z. Moreover, the beam ends, located at $x = 0$ and $x = L$, are restrained preventing any global rigid body motion. The Cartesian components of the displacement field of a Timoshenko nano-beam (u_1, u_2, u_3) is expressed by

$$u_1 = -z\varphi(x,t), \quad u_2 = 0, \quad u_3 = w(x,t) \tag{7}$$

Where $\varphi(x,t)$ is the cross-sectional rotation in the x-z plane and $w(x,t)$ is the transverse displacement at time t. The associated non-zero components of the strain field and of its derivative along the beam axis are then given by

$$\varepsilon_x^{(0)} = -z\frac{\partial\varphi}{\partial x}, \qquad \gamma_{xz}^{(0)} = -\varphi + \frac{\partial w}{\partial x}$$
$$\varepsilon_x^{(1)} = -z\frac{\partial^2\varphi}{\partial x^2}, \qquad \gamma_{xz}^{(1)} = -\frac{\partial\varphi}{\partial x} + \frac{\partial^2 w}{\partial x^2} \tag{8}$$

Let $M^{(0)}$ and $M^{(1)}$ be the dual fields of the bending curvature $\partial\varphi/\partial x$ and of its derivative along the beam axis $\partial^2\varphi/\partial x^2$, respectively. Also, $Q^{(0)}$ and $Q^{(1)}$ are defined as dual fields of the shear strain $\gamma_{xz}^{(0)}$ and of its derivative along the beam axis $\gamma_{xz}^{(1)}$, respectively.

Hellinger-Reissner's functional $\mathfrak{R}$ is introduced as [51,54].

$$\mathfrak{R} = \int_0^L \left[M^{(0)}\frac{\partial\varphi}{\partial x} + M^{(1)}\frac{\partial^2\varphi}{\partial x^2} + Q^{(0)}\left(-\varphi + \frac{\partial w}{\partial x}\right) + Q^{(1)}\left(-\frac{\partial\varphi}{\partial x} + \frac{\partial^2 w}{\partial x^2}\right) - \left(q^{(0)}w + q^{(1)}\frac{\partial w}{\partial x}\right) - \frac{1}{2I_E}\left((M^{(0)})^2 + \frac{1}{l_s^2}(M^{(1)})^2\right) - \frac{1}{2F_S A_G}\left((Q^{(0)})^2 + \frac{1}{l_s^2}(Q^{(1)})^2\right)\right]dx \tag{9}$$

where $q^{(0)}$ and $q^{(1)}$ are correspondingly dual fields of the transverse displacement w and of its derivative along the beam axis $\partial w/\partial x$ [15,55]. Furthermore, l_s designates gradient length-scale parameter introduced to establish the significance of the first-order strain gradient field. Timoshenko beam model also requires the introduction of a shear correction coefficient F_S accounting for non-uniform shear stress distribution through the thickness and depending on the cross-section geometry and Poisson's ratio [56]. The elasticity solution of Saint-Venant's problem [57–62] can be employed to set forth the formulation of shear correction coefficient.

While all of the displacement components and the stress resultants are selected as the primary variables subject to variation, performing the first-order variation of the aforementioned Hellinger-Reissner functional, followed by integration by parts, yields[1]

[1] An abstract treatment of variational principles, in the framework of continuum thermodynamics, can be found in Ref. [63].

The final version ofthis manuscript is available in COMPOSITES. PART B, ENGINEERING. DOI: 10.1016/j.compositesb.2018.07.036

FIG 1

$$\delta\Re = \int_0^L \left[\delta M^{(0)} \left(\frac{\delta\varphi}{\delta x} - \frac{M^{(0)}}{I_E} \right) + \delta M^{(1)} \left(\frac{\partial^2 \varphi}{\partial x^2} - \frac{M^{(1)}}{I_E l_s^2} \right) \right.$$
$$+ \delta Q^{(0)} \left(-\varphi + \frac{\delta w}{\delta x} - \frac{Q^{(0)}}{F_S A_G} \right) + \delta Q^{(1)} \left(-\frac{\delta\varphi}{\delta x} + \frac{\partial^2 w}{\partial x^2} - \frac{Q^{(1)}}{F_S A_G l_s^2} \right)$$
$$\left. - \delta w \left(\frac{\delta Q^{(0)}}{\delta x} - \frac{\partial^2 Q^{(1)}}{\partial x^2} + q^{(0)} - \frac{\delta q^{(1)}}{\delta x} \right) - \delta\varphi \left(\left(Q^{(0)} - \frac{\delta Q^{(1)}}{\delta x} \right) + \left(\frac{\delta M^{(0)}}{\delta x} - \frac{\partial^2 M^{(1)}}{\partial x^2} \right) \right) \right] dx$$
$$+ \left(Q^{(0)} - \frac{\partial Q^{(1)}}{\partial x} \right) \delta w \Big|_0^L + Q^{(1)} \left(\delta \frac{\delta w}{\delta x} - \delta\varphi \right) \Big|_0^L + M^{(1)} \delta \frac{\delta\varphi}{\delta x} \Big|_0^L + \left(M^{(0)} - \frac{\delta M^{(1)}}{\delta x} \right) \delta\varphi \Big|_0^L \tag{10}$$

To more simplify the first-order variation of the Hellinger-Reissner functional, analogous to the definition of the stress for 3D continuous bodies [15,55], flexural moment, shear force and distributed transverse load are introduced as

$$M = M^{(0)} - \frac{\partial M^{(1)}}{\partial x}, \qquad Q = Q^{(0)} - \frac{\partial Q^{(1)}}{\partial x}, \qquad q = q^{(0)} - \frac{\partial q^{(1)}}{\partial x} \tag{11}$$

As a result, the differential and boundary conditions of equilibrium of a strain gradient FG Timoshenko nano-beam may be determined by prescribing stationarity of Hellinger-Reissner functional $\delta\Re = 0$, while assuming arbitrary variations of curvature and shear strain fields

$$\begin{aligned}
&\delta w\text{: } \frac{\delta Q}{\partial x} + q = A_\rho \frac{\partial^2 w}{\partial t^2} \\
&\delta\varphi\text{: } \frac{\delta M}{\partial x} + Q = I_\rho \frac{\partial^2 \varphi}{\partial t^2} \\
&Q\delta w|_{x=0,L} = 0, \qquad M\delta\varphi|_{x=0,L} = 0 \\
&M^{(1)}|_{x=0,L} = 0, \qquad Q^{(1)}|_{x=0,L} = 0
\end{aligned} \tag{12}$$

where the effective cross-sectional mass A_ρ and rotatory inertia I_ρ are introduced in Eq. (6). Inertial forces in the dynamic form of the differential equation Eq. $(12)_1$ are taken into by following d'Alembert idea of adding correspondingly the inertial body force per unit length $(-A_\rho \partial^2 w/\partial t^2)$ to the distributed transverse load q and the inertial body moment per unit length $(I_\rho \partial^2 \varphi/\partial t^2)$ to the shear force Q [64]. As it is expected from the Hellinger-Reissner variational principle, the desired constitutive equations cast as ordinary differential equations and flexural moment shear force can be rewritten by virtue of Eq. (10) in the following form

$$\begin{aligned}
M &= M^{(0)} - \frac{\delta M^{(1)}}{\delta x} = \left(I_E \frac{\delta\varphi}{\delta x} \right) - \frac{\delta}{\delta x} \left(I_E l_s^2 \frac{\partial^2 \varphi}{\partial x^2} \right) = I_E \left(1 - l_s^2 \frac{\partial^2}{\partial x^2} \right) \frac{\delta\varphi}{\delta x} \\
Q &= Q^{(0)} - \frac{\partial Q^{(1)}}{\partial x} = F_S A_G \left(\frac{\partial w}{\partial x} - \varphi \right) - F_S A_G l_s^2 \frac{\partial}{\partial x} \left(\frac{\partial^2 w}{\partial x^2} - \frac{\delta\varphi}{\delta x} \right) \\
&= F_S A_G \left(1 - l_s^2 \frac{\partial^2}{\partial x^2} \right) \left(\frac{\partial w}{\partial x} - \varphi \right)
\end{aligned} \tag{13}$$

where bending stiffness I_E and shear area A_G are introduced in Eq. (5). The governing differential equations of a strain gradient FG Timoshenko nano-beam can be determined in terms of the deflection and rotation variables w and φ as

$$\begin{aligned}
&F_S A_G \left(1 - l_s^2 \frac{\partial^2}{\partial x^2} \right) \left(\frac{\partial^2 w}{\partial x^2} - \frac{\delta\varphi}{\delta x} \right) + q = A_\rho \frac{\partial^2 w}{\partial t^2} \\
&\left(1 - l_s^2 \frac{\partial^2}{\partial x^2} \right) \left(I_E \frac{\partial^2 \varphi}{\partial x^2} + F_S A_G \left(\frac{\partial w}{\partial x} - \varphi \right) \right) = I_\rho \frac{\partial^2 \varphi}{\partial t^2}
\end{aligned} \tag{14}$$

The set of differential and boundary conditions of equilibrium governing static and dynamic flexural behaviors of FG Timoshenko nano-beams in the framework of strain gradient theory of elasticity is the same as the established boundary-value problem in the literature by a formal application of Hamilton's principle [34,46,47].

However, in the case of Bernoulli-Euler beam theory $\varphi = \partial w/\partial x$ and thus $\gamma_{xz}^{(0)} = \gamma_{xz}^{(1)} = 0$. As a result, the governing differential and boundary conditions of equilibrium Eq. (12) degenerate to the corresponding boundary-value problem of a strain gradient FG Bernoulli-Euler nano-beam, while assuming arbitrary variations of curvature

$$\begin{aligned}
&\delta w\text{: } \frac{\partial^2 M}{\partial x^2} - q = I_E \left(1 - l_s^2 \frac{\partial^2}{\partial x^2} \right) \frac{\partial^4 w}{\partial x^4} - q = I_\rho \frac{\partial^4 w}{\partial x^2 \partial t^2} - A_\rho \frac{\partial^2 w}{\partial t^2} \\
&M\delta w_{,x}|_{x=0,L} = 0, \qquad \frac{\delta M}{\delta x} \delta w|_{x=0,L} = 0 \\
&M^{(1)}|_{x=0,L} = I_E \left(l_s^2 \frac{\partial^3 w}{\partial x^3} \right) \Big|_{x=0,L} = 0
\end{aligned} \tag{15}$$

4. Stress-driven nonlocal integral model of elasticity for FG Timoshenko nanobeams

A straight beam under flexure with the same geometry, material properties and coordinate system as introduced in the preceding section is considered here. According to Timoshenko kinematics Eq. (7), curvature $\varkappa(x)$ and shear strain $\gamma(x)$ are related to the transverse displacement $w(x)$ and the rotation of the cross-section $\varphi(x)$ by

$$\varkappa(x) = \frac{\partial\varphi}{\partial x}(x), \qquad \gamma(x) = \frac{\partial w}{\partial x}(x) - \varphi(x) \tag{16}$$

In the innovative nonlocal integral theory by G. Romano and R. Barretta [23,24], the nonlocal elastic strain field is got by convoluting the stress field with an averaging kernel. For Timoshenko nano-beams, elastic curvature $\varkappa$ and shear strain fields γ are introduced as outputs of integral convolutions between the local elastic curvature $C_E M$ and local elastic shear strain $C_G Q$ with an averaging kernel ψ dependent on a nonlocal parameter $\lambda > 0$ as

$$\begin{aligned}
\varkappa(x) &= \int_0^L \psi(x - y, \lambda) C_E M(y) dy \\
\gamma(x) &= \int_0^L \psi(x - y, \lambda) C_G Q(y) dy
\end{aligned} \tag{17}$$

with $x = 0$ and $x = L$ beam ends abscissas ands M and Q designate bending moment and shear force interactions, respectively. Also, C_E and C_G are the local elastic flexure and shear compliances defined by

$$C_E^{-1} = I_E, \qquad C_G^{-1} = F_S A_G \tag{18}$$

where bending stiffness I_E and shear area A_G are introduced in Eq. (5) and F_S is the shear correction coefficient [56]. Similar to Eringen's

The final version ofthis manuscript is available in COMPOSITES. PART B, ENGINEERING. DOI: 10.1016/j.compositesb.2018.07.036

strain-driven nonlocal integral model, the scalar kernel ψ fulfils the properties of symmetry and limit impulsivity [23,24].

$$\psi(x-y,\lambda)=\psi(y-x,\lambda)\geq 0, \qquad \lim_{\lambda\to 0^+}\psi(x,\lambda)=\delta(x) \tag{19}$$

where $\delta(x)$ is the Dirac distribution, corresponding to an unit impulse at the origin.

For one-dimensional nonlocal integral formulations, Helmholtz's special kernel is conveniently adapted [23,24].

$$\psi(x,\lambda)=\frac{1}{2l_c}\exp\left(-\frac{|x|}{l_c}\right) \tag{20}$$

with l_c nonlocal characteristic length defined by $l_c=\lambda L$, where L is the nano-beam length.

The output of the set of special integral constitutive laws introduced as Eq. (17) provides the unique set of solution of the constitutive differential equation [65].

$$\begin{aligned}\frac{M(x)}{l_c^2}&=I_E\left(\frac{\kappa(x)}{l_c^2}-\frac{\partial^2\kappa}{\partial x^2}(x)\right)\\ \frac{Q(x)}{l_c^2}&=F_SA_G\left(\frac{\gamma(x)}{l_c^2}-\frac{\partial^2\gamma}{\partial x^2}(x)\right)\end{aligned} \tag{21}$$

if and only if the following homogeneous higher-order constitutive boundary conditions, located at $x=0$ and $x=L$, are satisfied

$$\begin{aligned}&\frac{\partial\kappa}{\partial x}(0)-\frac{1}{l_c}\kappa(0)=0, \qquad \frac{\partial\kappa}{\partial x}(L)+\frac{1}{l_c}\kappa(L)=0\\ &\frac{\partial\gamma}{\partial x}(0)-\frac{1}{l_c}\gamma(0)=0, \qquad \frac{\partial\gamma}{\partial x}(L)+\frac{1}{l_c}\gamma(L)=0\end{aligned} \tag{22}$$

According to the FG Timoshenko beam model, differential and classical boundary conditions of dynamic equilibrium to be enforced write as

$$\begin{aligned}&\delta w:\ \frac{\partial Q}{\partial x}+q=A_\rho\frac{\partial^2 w}{\partial t^2}\\ &\delta\varphi:\ \frac{\partial M}{\partial x}+Q=I_\rho\frac{\partial^2\varphi}{\partial t^2}\\ &Q\delta w|_{x=0,L}=0, \qquad M\delta\varphi|_{x=0,L}=0\end{aligned} \tag{23}$$

where the effective cross-sectional mass A_ρ and rotatory inertia I_ρ are introduced in Eq. (6). Enforcement of the differential conditions of kinematic compatibility Eq. (16) provides the dynamic differential equation governing flexure of FG Timoshenko nano-beams in terms of deflection and rotation fields w and φ as

$$\begin{aligned}&F_SA_G\left(\frac{1}{l_c^2}-\frac{\partial^2}{\partial x^2}\right)\left(\frac{\partial^2 w}{\partial x^2}-\frac{\partial\varphi}{\partial x}\right)+\frac{q}{l_c^2}=\frac{A_\rho}{l_c^2}\frac{\partial^2 w}{\partial t^2}\\ &\left(\frac{1}{l_c^2}-\frac{\partial^2}{\partial x^2}\right)\left(I_E\frac{\partial^2\varphi}{\partial x^2}+F_SA_G\left(\frac{\partial w}{\partial x}-\varphi\right)\right)=\frac{I_\rho}{l_c^2}\frac{\partial^2\varphi}{\partial t^2}\end{aligned} \tag{24}$$

It can be inferred from Eq. (24) that the set of differential equations governing FG Timoshenko nano-beams for both the stress-driven nonlocal integral model and the strain gradient theory of elasticity are the same provided that the gradient length-scale parameter l_s is replaced with the nonlocal characteristic length l_c. Such an assumption is feasible only for positive values of the nonlocal characteristic length l_c. Indeed, while in the strain gradient theory it is possible to set the gradient length-scale parameter $l_s=0$, the stress-driven nonlocal model equipped with the bi-exponential kernel Eq. (20) is not defined when the characteristic length is vanishing. Only a limit evaluation as l_c tends to zero is permissible.

Nevertheless, there exist profound differences in the assumptions between the stress-driven nonlocal integral model and strain gradient theory. The strain gradient theory of elasticity is fundamentally established on the postulate that the material response at a point is dependent not only on the local strain, but also on the strain gradients of various order, up to a value characterizing the non-simplicity grade of the material and the expected extent of physics to be captured [16,17]. However, in the stress-driven fully nonlocal theory the elastic strain field is presumed to be an integral convolution of the stress field in the continuum. Furthermore, while the differential equation stemming from the stress-driven nonlocal approach is identical to the one exposed in the context of a strain-gradient model of elasticity (for positive characteristic parameters), the required higher-order boundary conditions are completely different.

Once more, in the case of Bernoulli-Euler beam theory $\varphi=\partial w/\partial x$ and thus $\gamma=0$. Consequently, the constitutive differential equation Eq. $(21)_1$ and constitutive boundary conditions Eq. $(22)_1$ degenerate to the corresponding constitutive boundary-value problem of FG Bernoulli-Euler nano-beams, provided that the elastic curvature is substituted by $\kappa=\partial^2 w/\partial x^2$.

5. Free vibration analysis

The differences in free vibration analysis associated with the stress-driven nonlocal integral model and the strain gradient theory of elasticity are illustrated through the examination of vibrating nano-beam problem with the Timoshenko kinematics. The differential conditions of dynamic equilibrium, Eq. (14) or Eq. (24), can be also uncoupled employing some straightforward mathematics. To get the uncoupled differential equation for the rotation φ, the second equation of dynamic equilibrium, Eq. $(14)_2$ or Eq. $(24)_2$, should be first solved for transverse displacement w in terms of the rotation and its higher-order derivatives. Differentiating first equation of dynamic equilibrium, Eq. $(14)_1$ or Eq. $(24)_1$, with respect to x and then substituting from the resulted equation for transverse displacement w, on rearranging terms, the desired uncoupled differential equation for the rotation φ can be obtained. Following the similar mathematical procedure for transverse displacement w, the uncoupled differential conditions of dynamic equilibrium are obtained

$$\begin{aligned}&\left(1-l^2\frac{\partial^2}{\partial x^2}\right)\left[\left(1-l^2\frac{\partial^2}{\partial x^2}\right)\left(I_E\frac{\partial^4 w}{\partial x^4}\right)-\left(1-\frac{I_E}{F_SA_G}\frac{\partial^2}{\partial x^2}\right)\left(q-A_\rho\frac{\partial^2 w}{\partial t^2}\right)-I_\rho\frac{\partial^4 w}{\partial x^2\partial t^2}\right]\\ &\quad=\frac{I_\rho}{F_SA_G}\frac{\partial^2 q}{\partial t^2}-\frac{I_\rho A_\rho}{F_SA_G}\frac{\partial^4 w}{\partial t^4}\\ &\left(1-l^2\frac{\partial^2}{\partial x^2}\right)\left[\left(1-l^2\frac{\partial^2}{\partial x^2}\right)\left(I_E\frac{\partial^4\varphi}{\partial x^4}\right)-\frac{\partial q}{\partial x}+A_\rho\frac{\partial^2\varphi}{\partial t^2}-\left(I_\rho+\frac{I_EA_\rho}{F_SA_G}\right)\frac{\partial^4\varphi}{\partial x^2\partial t^2}\right]=-\frac{I_\rho A_\rho}{F_SA_G}\frac{\partial^4\varphi}{\partial t^4}\end{aligned} \tag{25}$$

where l is a positive characteristic length, $l=l_s$ gradient length-scale parameter and $l=l_c>0$ nonlocal characteristic length, in the framework of strain gradient theory of elasticity and stress-driven nonlocal integral model, respectively.

For free vibration analyses, the applied distributed loading terms vanish. Also, natural frequencies and mode shapes of vibrations may be determined with the aid of separation of spatial and time variables as [66].

$$w(x,t)=W(x)\exp(i\omega t), \qquad \varphi(x,t)=\Phi(x)\exp(i\omega t) \tag{26}$$

with $i=\sqrt{-1}$ and ω is the natural frequency of vibrations. Substitution of the aforementioned separation of variables into the governing equation (25) leads to the same governing equation for either flexural deflection base function $W(x)$ or rotation base functions $\Phi(x)$ as

$$\begin{aligned}&\left(1-l^2\frac{d^2}{dx^2}\right)\left[\left(1-l^2\frac{d^2}{dx^2}\right)\left(I_E\frac{d^4\Upsilon}{dx^4}\right)+\left(\frac{A_\rho I_E}{F_SA_G}+I_\rho\right)\omega^2\frac{d^2\Upsilon}{dx^2}-\omega^2A_\rho\Upsilon\right]\\ &\quad+\frac{I_\rho A_\rho}{F_SA_G}\omega^4\Upsilon=0\end{aligned} \tag{27}$$

where $\Upsilon(x)$ may be replaced with either base functions $W(x)$ or $\Phi(x)$. The analytical solution of the preceding equation governing the spatial base functions can be expressed by

$$W(x)=\sum_{k=1}^{8}W_k\exp(\zeta_k x), \qquad \Phi(x)=\sum_{k=1}^{8}\Phi_k\exp(\zeta_k x) \tag{28}$$

where W_k, Φ_k $(k=1..8)$ are unknown constants needed to be determined by suitable boundary conditions, along with ζ_k that are the roots of the

The final version ofthis manuscript is available in COMPOSITES. PART B, ENGINEERING. DOI: 10.1016/j.compositesb.2018.07.036

following characteristic equation

$$\left(\frac{I_\rho A_\rho}{F_S A_G}\omega^2 - A_\rho\right)\omega^2 + \left(\left(\frac{A_\rho I_E}{F_S A_G} + I_\rho\right) + l^2 A_\rho\right)\omega^2\zeta^2 + \left(I_E - l^2\left(\frac{A_\rho I_E}{F_S A_G} + I_\rho\right)\omega^2\right)\zeta^4 - (2l^2 I_E)\zeta^6 + (l^4 I_E)\zeta^8 = 0 \tag{29}$$

However, the unknown constants W_k, $\Phi_k (k = 1..8)$ are not independent and can be related to each other employing Eq. $(14)_1$ or Eq. $(24)_1$ by virtue of Eqs. (26) and (28) as

$$\left(\zeta_k^2 - l^2\zeta_k^4 + \frac{A_\rho\omega^2}{F_S A_G}\right)W_k = \Phi_k(\zeta_k - l^2\zeta_k^3) \tag{30}$$

To numerically assess the fundamental natural frequency of Timoshenko nano-beam, four different set of boundary conditions including simply-supported, clamped-simply supported, doubly-clamped and cantilever are considered. For each set of boundary conditions, a homogeneous algebraic system in terms of the unknown constants $W_k (k = 1..8)$ can be found by employing the abovementioned boundary conditions in the solution form of the spatial base function as Eq. (28). It is known that to obtain a non-trivial solution, the system of algebraic equations should be singular, and consequently, the determinant of the coefficients of the homogeneous algebraic system should vanish. As a result, this solution procedure leads to the highly nonlinear characteristic equation for each set of boundary conditions in terms of the fundamental natural frequency that should be numerically solved.

Also for consistency, in all of the illustrative results, the subsequent dimensionless fundamental natural frequency ϖ is introduced

$$\varpi^2 = \omega^2 L^4 \frac{\rho_1 A}{E_1 I_y} \tag{31}$$

Prior to performing the parametric study of free vibration analysis of FG Timoshenko nano-beams, the fundamental natural frequency of an elastically homogeneous Bernoulli-Euler nano-beam is examined. The vibration results for Bernoulli-Euler nano-beams based on the stress-driven nonlocal integral model, recently contributed by Apuzzo et al. [30], are recovered as a special case. The effect of rotatory inertia is ignored in the results contributed by Apuzzo et al. [30] but examined in the present study according to Eq. (15). As a result, the fundamental natural frequency is determined in terms of both the dimensionless nonlocal parameter λ and the aspect ratio L/h of Bernoulli-Euler nano-beam.

The effects of the nano-beam aspect ratio L/h on the dimensionless fundamental natural frequency of elastically homogeneous Bernoulli-Euler nano-beams associated with the strain gradient theory of elasticity (SGT) and the stress-driven nonlocal integral model (SDM) are provided in Figs. 2–5 for simply-supported, clamped-simply supported, doubly-clamped and cantilever boundary conditions, respectively. While the aspect ratio L/h is assumed to range in the set {10,20, ∞}, the dimensionless characteristic parameter λ is ranging in the interval]0,0.1[. In all illustrative examples, the acronyms SS, CS, CC and CF stand for simply-supported, clamped-simply supported, doubly-clamped and cantilever, respectively. As it can be observed from Figs. 2–5, for large aspect ratio L/h there is slight difference between the results of Apuzzo et al. [30] and that which includes rotatory inertia. However, for stubby nano-beams, the rotatory inertia effects can be significant. Also, while the fundamental natural frequencies of Bernoulli-Euler nano-beams with SS, CS and CC ends underestimate the counterpart results of Apuzzo et al. [30], the fundamental natural frequencies of nano-beams with CF ends overestimate them. Numerical evaluations of dimensionless fundamental natural frequency $\varpi(\lambda)$ evaluated by the stress-driven nonlocal integral model and the strain gradient theory of elasticity are tabulated in Tables 1–4 for simply-supported, clamped-simply supported, doubly-clamped and cantilever boundary conditions, respectively.

FIG. 2

FIG. 3

FIG. 4

In Figs. 6–9, the effect of the aspect ratio L/h on the dimensionless fundamental natural frequency ϖ is demonstrated for SS, CS, CC and CF boundary conditions, respectively. The power-law exponent, elastic modulus ratio, material density ratio and dimensionless characteristic parameter are set to be $n = 1$, $E_2/E_1 = 1/4$, $\rho_2/\rho_1 = 1/2$ and $\lambda = 0.1$. As demonstrated in Figs. 6–9, dimensionless fundamental natural frequencies according to the strain gradient theory of elasticity (SGT) underestimate the counterpart results based on the stress-driven

The final version ofthis manuscript is available in COMPOSITES. PART B, ENGINEERING. DOI: 10.1016/j.compositesb.2018.07.036

FIG. 5

Table 1
Fundamental natural frequency of a simply supported isotropic Bernoulli-Euler nano-beam versus the characteristic parameter λ.

ϖ

λ	$L/h = 10$		$L/h = 20$		Apuzzo et al. [30]	
	SDM	SGT	SDM	SGT	SDM	SGT
0^+	9.82927	9.82927	9.85947	9.85947	9.8696	9.8696
0.01	9.83402	9.83392	9.86424	9.86414	9.87438	9.87428
0.02	9.84787	9.8471	9.87814	9.87736	9.88829	9.88751
0.03	9.87022	9.86761	9.90055	9.89794	9.91072	9.90811
0.04	9.90042	9.89427	9.93084	9.92468	9.94105	9.93487
0.05	9.93783	9.9259	9.96837	9.95641	9.97861	9.96664
0.06	9.98183	9.9614	10.0125	9.99201	10.0228	10.0023
0.07	10.0318	9.9997	10.0626	10.0304	10.0729	10.0407
0.08	10.0871	10.0398	10.1181	10.0707	10.1285	10.0811
0.09	10.1472	10.081	10.1784	10.112	10.1888	10.1224
0.1	10.2115	10.1223	10.2429	10.1535	10.2534	10.1639

Table 2
Fundamental natural frequency of a clamped-simply supported isotropic Bernoulli-Euler nano-beam versus the characteristic parameter λ.

ϖ

λ	$L/h = 10$		$L/h = 20$		Apuzzo et al. [30]	
	SDM	SGT	SDM	SGT	SDM	SGT
0^+	15.3448	15.3448	15.3997	15.3997	15.4182	15.4182
0.01	15.5104	15.3649	15.5665	15.42	15.5854	15.4385
0.02	15.7016	15.4229	15.7589	15.4783	15.7781	15.4969
0.03	15.9176	15.5151	15.9761	15.571	15.9958	15.5897
0.04	16.1574	15.6383	16.2172	15.6947	16.2373	15.7137
0.05	16.4199	15.7893	16.4811	15.8465	16.5016	15.8657
0.06	16.7038	15.9651	16.7664	16.0232	16.7874	16.0427
0.07	17.0076	16.1631	17.0716	16.2221	17.0931	16.2419
0.08	17.3298	16.3805	17.3954	16.4405	17.4174	16.4606
0.09	17.6689	16.6149	17.736	16.676	17.7586	16.6965
0.1	18.0235	16.8641	18.0921	16.9264	18.1152	16.9473

nonlocal integral model (SDM) for both Timoshenko beam model (TM) and Bernoulli-Euler beam model (BEM). Moreover, difference between Timoshenko and Bernoulli-Euler nano-beam model tend to vanish for increasing values of the aspect ratio L/h. Numerical evaluations of dimensionless fundamental natural frequency $\varpi(L/h)$ associated with the stress-driven nonlocal integral model and the strain gradient theory of elasticity are tabulated in Table 5 for SS, CS, CC and CF boundary conditions, respectively.

Table 3
Fundamental natural frequency of a doubly clamped isotropic Bernoulli-Euler nano-beam versus the characteristic parameter λ.

ϖ

λ	$L/h = 10$		$L/h = 20$		Apuzzo et al. [30]	
	SDM	SGT	SDM	SGT	SDM	SGT
0^+	22.2594	22.2594	22.3447	22.3447	22.3733	22.3733
0.01	22.7334	22.3126	22.8221	22.3981	22.8518	22.4268
0.02	23.2701	22.4657	23.3622	22.5521	23.3932	22.5812
0.03	23.8697	22.7111	23.9654	22.7989	23.9976	22.8284
0.04	24.5316	23.0424	24.6309	23.1319	24.6643	23.1619
0.05	25.2541	23.454	25.3572	23.5454	25.3918	23.5762
0.06	26.0346	23.9408	26.1415	24.0345	26.1775	24.066
0.07	26.87	24.498	26.9808	24.5943	27.0181	24.6266
0.08	27.7564	25.121	27.8713	25.22	27.9099	25.2532
0.09	28.6899	25.805	28.8089	25.907	28.8489	25.9412
0.1	29.6662	26.5456	29.7894	26.6508	29.8309	26.6861

Table 4
Fundamental natural frequency of a cantilever isotropic Bernoulli-Euler nano-beam versus the characteristic parameter λ.

ϖ

λ	$L/h = 10$		$L/h = 20$		Apuzzo et al. [30]	
	SDM	SGT	SDM	SGT	SDM	SGT
0^+	3.51727	3.51727	3.51633	3.51633	3.51602	3.51602
0.01	3.55281	3.51808	3.55185	3.51713	3.55153	3.51682
0.02	3.58905	3.52045	3.58806	3.51949	3.58773	3.51918
0.03	3.62597	3.52429	3.62495	3.52333	3.62461	3.52301
0.04	3.66352	3.52954	3.66247	3.52856	3.66212	3.52824
0.5	3.70169	3.5361	3.7006	3.53511	3.70024	3.53478
0.06	3.74041	3.5439	3.73928	3.5429	3.73891	3.54256
0.07	3.77964	3.55286	3.77847	3.55183	3.77808	3.55149
0.08	3.81934	3.56289	3.81812	3.56184	3.81771	3.56149
0.09	3.85943	3.57391	3.85816	3.57283	3.85774	3.57247
0.1	3.89988	3.58583	3.89855	3.58471	3.89811	3.58434

FIG. 6

$\lambda = 0.1$, $E_2/E_1 = 1/4$, $n = 1$, $\rho_2/\rho_1 = 1/2$.

Figs. 10–13 provide the effect of the elastic moduli ratio E_2/E_1 on the dimensionless fundamental natural frequency ϖ for SS, CS, CC and CF boundary conditions, respectively. The dimensionless characteristic parameter, power-law exponent, material density ratio and the aspect ratio are given by $\lambda = 0.1$, $n = 1$, $\rho_2/\rho_1 = 1/2$ and $L/h = 10$. The dimensionless fundamental natural frequency of the FG Bernoulli-Euler and Timoshenko nano-beam increase as values of the elastic moduli ratio E_2/E_1 increases. As before, the fundamental natural frequency of the strain gradient theory of elasticity is always less than the results of

The final version ofthis manuscript is available in COMPOSITES. PART B, ENGINEERING. DOI: 10.1016/j.compositesb.2018.07.036

FIG. 7

FIG. 8

FIG. 9

Table 5
Fundamental natural frequency of a nano-beam versus the aspect ratio L/h for $\lambda = 0.1$, $E_2/E_1 = 1/4$, $n = 1$, $\rho_2/\rho_1 = 1/2$.

Boundary Conditions	ϖ				
	L/h	Bernoulli-Euler		Timoshenko	
		SDM	SGT	SDM	SGT
Simply-Supported	5	8.64462	8.5691	8.3568	8.22957
	10	8.74593	8.66957	8.66693	8.57572
	15	8.76509	8.68857	8.72933	8.64602
	20	8.77182	8.69525	8.75158	8.67115
	25	8.77495	8.69834	8.76195	8.68287
	30	8.77664	8.70003	8.7676	8.68926
Clamped-Simply	5	15.2165	14.2439	13.5244	12.6427
	10	15.4373	14.4442	14.9302	13.9646
	15	15.4792	14.4822	15.2451	14.2608
	20	15.4939	14.4956	15.3605	14.3694
	25	15.5008	14.5018	15.4148	14.4205
	30	15.5045	14.5052	15.4446	14.4485
Doubly Clamped	5	25.0146	22.3992	19.8936	17.9004
	10	25.4098	22.7367	23.6777	21.2291
	15	25.485	22.8009	24.6601	22.0847
	20	25.5115	22.8235	25.0354	22.4106
	25	25.5237	22.834	25.2154	22.5666
	30	25.5304	22.8396	25.3148	22.6528
Cantilever	5	3.34397	3.07437	3.2374	2.98244
	10	3.3396	3.07067	3.31191	3.04684
	15	3.33879	3.06999	3.32639	3.05933
	20	3.33851	3.06975	3.33152	3.06374
	25	3.33838	3.06964	3.3339	3.06579
	30	3.33831	3.06958	3.33519	3.06691

FIG. 10

the stress-driven nonlocal integral model. Also, the numerical results of dimensionless fundamental natural frequency $\varpi(E_2/E_1)$ according to the stress-driven nonlocal integral model and the strain gradient theory of elasticity are tabulated in Table 6 for SS, CS, CC and CF boundary conditions, respectively.

The dimensionless fundamental natural frequency ϖ of FG Bernoulli-Euler and Timoshenko nano-beams versus the power-law exponent n is examined in Figs. 14–17 for SS, CS, CC and CF boundary conditions, respectively. The dimensionless characteristic parameter, elastic moduli ratio, material density ratio and the aspect ratio is assumed as $\lambda = 0.1$, $E_2/E_1 = 1/4$, $\rho_2/\rho_1 = 1/2$ and $L/h = 10$. As the power-law exponent varies from 0 to ∞, the elastic material properties change from the material properties of constituents 1 to constituents 2, respectively. Since the elastic moduli ratio is assumed as $E_2/E_1 = 1/4$, the dimensionless fundamental natural frequency increases for increasing values of the power-law exponent n. Numerical evaluations of dimensionless fundamental natural frequency $\varpi(n)$ determined employing the stress-driven nonlocal integral model and the strain gradient theory of elasticity are tabulated in Table 7 for SS, CS, CC and CF boundary conditions, respectively.

Influences of the material density ratio ρ_2/ρ_1 on the dimensionless fundamental natural frequency ϖ corresponding to the stress-driven nonlocal integral and the strain gradient models are provided in

The final version ofthis manuscript is available in COMPOSITES. PART B, ENGINEERING. DOI: 10.1016/j.compositesb.2018.07.036

FIG 11

FIG 12

FIG 13

Table 6
Fundamental natural frequency of a nano-beam versus the elastic modulus ratio E_2/E_1 for $\lambda = 0.1$, $L/h = 10$, $n = 1$, $\rho_2/\rho_1 = 1/2$.

Boundary Conditions	ϖ				
	E_2/E_1	Bernoulli-Euler		Timoshenko	
		SDM	SGT	SDM	SGT
Simply-Supported	1/4	8.74593	8.66957	8.66693	8.57572
	1/2	10.0221	9.93463	9.92319	9.81712
	1	11.793	11.69	11.6722	11.5465
	2	14.1734	14.0497	14.0335	13.8835
	4	17.4919	17.3391	17.3339	17.1514
Clamped-Simply	1/4	15.4373	14.4442	14.9302	13.9646
	1/2	17.6898	16.5519	17.0568	15.9531
	1	20.8156	19.4766	20.0436	18.7463
	2	25.0172	23.4079	24.122	22.5611
	4	30.8745	28.8884	29.8605	27.9292
Doubly Clamped	1/4	25.4098	22.7367	23.6777	21.2291
	1/2	29.1176	26.0544	26.9652	24.1804
	1	34.2625	30.6582	31.643	28.377
	2	41.1784	36.8466	38.1346	34.1962
	4	50.8196	45.4734	47.3555	42.4581
Cantilever	1/4	3.3396	3.07067	3.31191	3.04684
	1/2	3.82691	3.51874	3.79309	3.48965
	1	4.50311	4.1405	4.46223	4.10531
	2	5.41207	4.97626	5.36425	4.9351
	4	6.6792	6.14135	6.62381	6.09369

FIG 14

FIG 15

Figs. 18–21 for SS, CS, CC and CF boundary conditions, respectively. The dimensionless characteristic parameter, elastic modulus ratio, power-law exponent and the aspect ratio are given by $\lambda = 0.1$, $E_2/E_1 = 1/4$, $n = 1$ and $L/h = 10$. As it can be observed from Figs. 18–21, the fundamental natural frequency of FG Bernoulli-Euler and Timoshenko nano-beams tend to decrease depending on the increase in the material density ratio. Also, the numerical results of dimensionless fundamental natural frequency $\varpi(\rho_2/\rho_1)$ according to the stress-driven nonlocal integral model and the strain gradient theory of

The final version ofthis manuscript is available in COMPOSITES. PART B, ENGINEERING. DOI: 10.1016/j.compositesb.2018.07.036

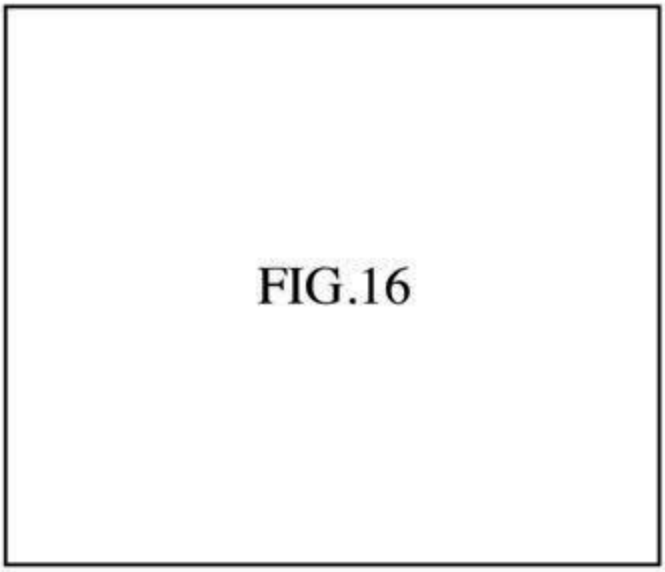

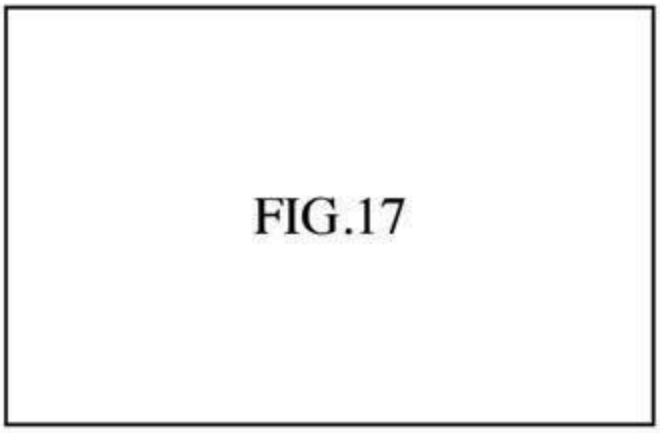

elasticity are tabulated in Table 8 for SS, CS, CC and CF boundary conditions, respectively.

Figs. 22–25 depict the plots of the dimensionless fundamental natural frequency ϖ associated with the stress-driven nonlocal integral model and the strain gradient theory of elasticity versus the dimensionless characteristic parameter λ, for both Timoshenko and Bernoulli-Euler beam models while SS, CS, CC and CF boundary conditions are imposed, respectively. As the elastic modulus ratio, power-law exponent, material density ratio and the aspect ratio are given by E_2/E_1, $n = 1$, $\rho_2/\rho_1 = 1/2$ and $L/h = 10$, the dimensionless characteristic parameter λ is assumed to range in the set $]0,0.1[$. It is noticeably deduced from Figs. 22–25 that both the stress-driven nonlocal integral model and the strain gradient theory of elasticity exhibit a hardening behavior in terms of the dimensionless characteristic parameter. However, the hardening effect of the stress-driven nonlocal model is more noticeable in comparison to the strain gradient theory. While both size-dependent models provide the results of local beam theory for vanishing dimensionless characteristic parameter $\lambda \to 0$, discrepancy between the natural frequencies of two size-dependent models is enhanced by increasing values of the dimensionless characteristic parameter. Finally, the results of fundamental natural frequency according to the Bernoulli-Euler beam theory overestimate the fundamental natural frequencies of the Timoshenko beam model. Also, the numerical results of dimensionless fundamental natural frequency $\varpi(\lambda)$ according to the stress-driven nonlocal integral model and the strain gradient theory of elasticity are tabulated in Table 9 for SS, CS, CC and CF boundary conditions, respectively.

The effect of different sets of boundary conditions on the

Table 7
Fundamental natural frequency of a nano-beam versus power-law exponent n for $\lambda = 0.1$, $L/h = 10$, $E_2/E_1 = 1/4$, $\rho_2/\rho_1 = 1/2$.

Boundary Conditions	ϖ				
	n	Bernoulli-Euler		Timoshenko	
		SDM	SGT	SDM	SGT
Simply-Supported	0	7.22063	7.15758	7.14668	7.06977
	1	8.74593	8.66957	8.66693	8.57572
	2	8.93397	8.85597	8.85594	8.76326
	5	9.29107	9.20995	9.20833	9.11166
	10	9.59727	9.51347	9.50816	9.40763
	∞	10.21151	10.12235	10.10693	9.998166
Clamped-Simply	0	12.7445	11.9247	12.2721	11.4779
	1	15.4373	14.4442	14.9302	13.9646
	2	15.7697	14.7552	15.2683	14.2809
	5	16.4001	15.345	15.8689	14.8425
	10	16.9403	15.8505	16.369	15.3101
	∞	18.0235	16.8641	17.3554	16.2322
Doubly Clamped	0	20.9772	18.7706	19.3744	17.3748
	1	25.4098	22.7367	23.6777	21.2291
	2	25.9573	23.2265	24.2416	21.7332
	5	26.9951	24.155	25.1788	22.5741
	10	27.8841	24.9506	25.935	23.2539
	∞	29.6662	26.5456	27.3996	24.5717
Cantilever	0	2.75763	2.53556	2.5	2.5138
	1	3.3396	3.07067	3.31191	3.04684
	2	3.41089	3.13623	3.38356	3.11271
	5	3.5471	3.26147	3.51836	3.23674
	10	3.6643	3.36923	3.63353	3.34276
	∞	3.89988	3.58583	3.86411	3.55505

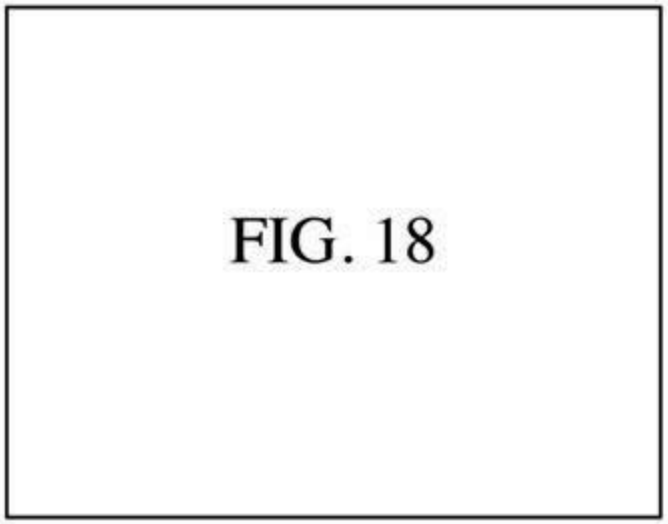

dimensionless fundamental natural frequency ϖ of FG Bernoulli-Euler and Timoshenko nano-beams evaluated by the stress-driven nonlocal integral model and the strain gradient theory of elasticity versus the dimensionless characteristic parameter λ is shown in Figs. 26 and 27, respectively. The elastic moduli ratio, power-law exponent, material density ratio and the aspect ratio are given by $E_2/E_1 = 1/4$, $n = 1$, $\rho_2/\rho_1 = 1/2$ and $L/h = 10$. As demonstrated in Figs. 26 and 27, both the stress-driven nonlocal integral model and the strain gradient theory of elasticity reveal a hardening behavior both in terms of the dimensionless characteristic parameter λ and of the number of kinematic boundary constraints. As expected [30], the softest structural response with respect to the considered boundary conditions is revealed by cantilever nano-beams.

The final version ofthis manuscript is available in COMPOSITES. PART B, ENGINEERING. DOI: 10.1016/j.compositesb.2018.07.036

FIG. 19

FIG. 20

FIG. 21

Table 8
Fundamental natural frequency of a nano-beam versus the density ratio ρ_2/ρ_1 for $\lambda = 0.1$, $L/h = 10$, $E_2/E_1 = 1/4$, $n = 1$.

Boundary Conditions	ϖ				
	ρ_2/ρ_1	Bernoulli-Euler		Timoshenko	
		SDM	SGT	SDM	SGT
Simply-Supported	1/4	9.58394	9.50026	9.49724	9.05774
	1/2	8.74593	8.66957	8.66693	8.57572
	1	7.57306	7.50694	7.50468	7.42571
	2	6.18431	6.13031	6.12844	6.06395
	4	4.79197	4.75013	4.74862	4.69864
Clamped-Simply	1/4	16.9178	15.8293	16.3614	15.303
	1/2	15.4373	14.4442	14.9302	13.9646
	1	13.3666	12.5068	12.9278	12.0917
	2	10.9158	10.2136	10.5573	9.87445
	4	8.45888	7.91463	8.18069	7.65148
Doubly Clamped	1/4	27.8477	24.9177	25.9466	23.263
	1/2	25.4098	22.7367	23.6777	21.2291
	1	22.001	19.6867	20.5024	18.3822
	2	17.9674	16.0773	16.7427	15.0112
	4	13.9239	12.4588	12.9733	11.6315
Cantilever	1/4	3.65821	3.36364	3.62863	3.33819
	1/2	3.3396	3.07067	3.31191	3.04684
	1	2.89222	2.65932	2.86798	2.63845
	2	2.36145	2.17129	2.34187	2.15444
	4	1.8291	1.68182	1.81432	1.66909

FIG. 22

FIG. 23

6. Concluding remarks

The elastodynamic problems of functionally graded (FG) Timoshenko straight nano-beams have been formulated by strain gradient and stress-driven nonlocal theories of elasticity. Rectangular cross-sections have been examined. Material density and Euler-Young modulus have been assumed to vary only along the bending axis (thickness) according to a power law. Size-dependent free vibrations of FG slender and stubby nano-beams have been analytically investigated

The final version ofthis manuscript is available in COMPOSITES. PART B, ENGINEERING. DOI: 10.1016/j.compositesb.2018.07.036

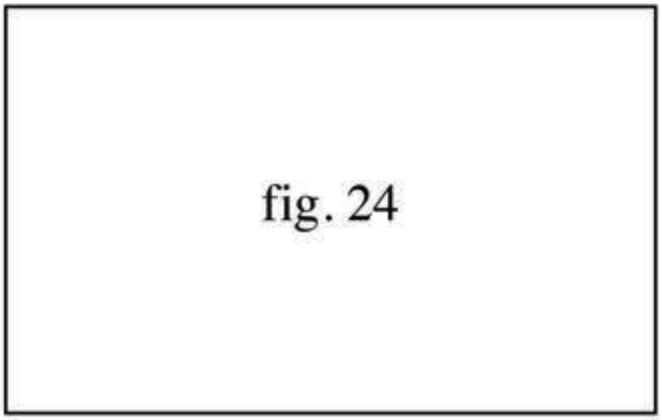

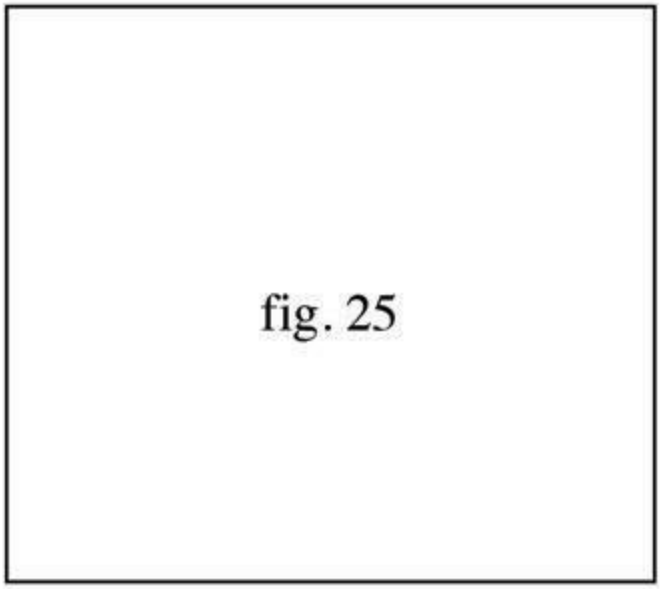

for different kinematic boundary conditions of engineering interest.

The main outcomes of the present study may be summarized as follows.

- The through-thickness functional variation of material properties significantly affects vibrational responses of nano-beams. Natural frequencies can be thus controlled by tailoring appropriately the material properties.
- A hardening behavior of the natural frequencies in terms of the small-scale parameter has been pointed out for both stress-driven nonlocal and strain gradient models.
- For both FG Timoshenko and Bernoulli-Euler nano-beams, strain gradient theory of elasticity underestimates the natural frequencies associated with stress-driven nonlocal theory.
- Fundamental natural frequencies increase with the increase of scale parameters.
- As the small-scale parameter tends to zero, natural frequencies determined by both strain gradient and stress-driven nonlocal models coincide with the local ones.
- The discrepancy between the vibrational results corresponding to stress-driven nonlocal and strain gradient theories increases as the small-scale parameter increases.
- While the effects of transverse shear deformation are noteworthy for small values of aspect ratio, the gap between the vibrational responses of FG Timoshenko and Bernoulli-Euler nano-beams tends to vanish for increasing values of the aspect ratio.
- The effect of the rotatory inertia on the fundamental natural

Table 9
Fundamental natural frequency of a nano-beam versus the characteristic parameter λ for $L/h = 10$, $E_2/E_1 = 1/4$, $n = 1$, $\rho_2/\rho_1 = 1/2$.

Boundary Conditions	ϖ				
	λ	Bernoulli-Euler		Timoshenko	
		SDM	SGT	SDM	SGT
Simply-Supported	0^+	8.41855	8.41855	8.32418	8.32418
	0.02	8.43449	8.43383	8.34366	8.33932
	0.04	8.47949	8.47423	8.39192	8.37946
	0.06	8.54922	8.53172	8.46467	8.43685
	0.08	8.63937	8.59891	8.55767	8.50429
	0.1	8.74593	8.66957	8.66693	8.57572
Clamped-Simply	0^+	13.1428	13.1428	12.7475	12.7475
	0.02	13.4485	13.2097	13.0394	12.81
	0.04	13.8389	13.3942	13.4115	12.9824
	0.06	14.3069	13.6742	13.8568	13.2442
	0.08	14.8431	14.0299	14.3663	13.5769
	0.1	15.4373	14.4442	14.9302	13.9646
Doubly Clamped	0^+	19.0654	19.0654	18.0617	18.0617
	0.02	19.9312	19.2421	18.8378	18.2161
	0.04	21.0118	19.7361	19.8011	18.6467
	0.06	22.2992	20.5056	20.9424	19.3143
	0.08	23.774	21.5165	22.2428	20.1855
	0.1	25.4098	22.7367	23.6777	21.2291
Cantilever	0^+	3.01197	3.01197	2.98919	2.98919
	0.02	3.07344	3.01469	3.04973	2.99186
	0.04	3.13721	3.02247	3.11254	2.99951
	0.06	3.20305	3.03478	3.17739	3.0116
	0.08	3.27063	3.05103	3.24397	3.02757
	0.1	3.3396	3.07067	3.31191	3.04684

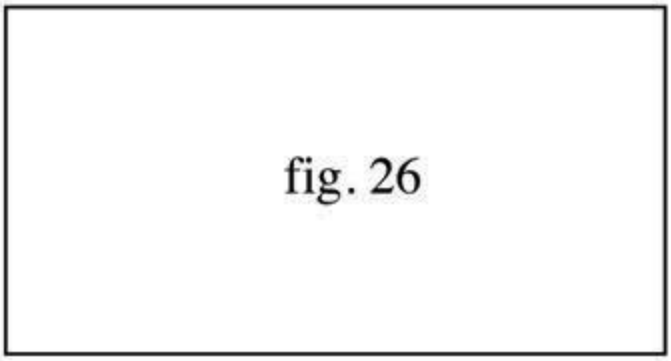

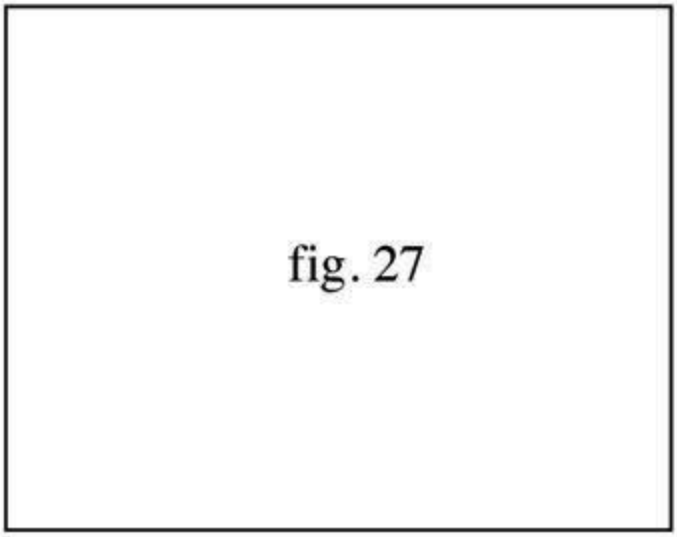

The final version ofthis manuscript is available in COMPOSITES. PART B, ENGINEERING. DOI: 10.1016/j.compositesb.2018.07.036

frequencies of Bernoulli-Euler nano-beams predicted by either of size-dependent models is more significant for lower aspect ratios.

As a final comment, it can be concluded that the stress-driven nonlocal integral model provides an effective approach to characterize size-dependent vibrational behavior of FG Timoshenko nano-beams. The contributed results could be conveniently employed for the design of modern stubby beam-like components of Nano-Electro-Mechanical Systems.

Appendix A. Supplementary data

Supplementary data related to this article can be found at https://doi.org/10.1016/j.compositesb.2018.07.036.

References

[1] Aifantis EC. Internal length gradient (ILG) material mechanics across scales and disciplines. Adv Appl Mech 2016;49:1–110. https://doi.org/10.1016/bs.aams.2016.08.001.

[2] Rafii-Tabar H, Ghavanloo E, Fazelzadeh SA. Nonlocal continuum-based modeling of mechanical characteristics of nanoscopic structures. Phys Rep 2016;638:1–97. https://doi.org/10.1016/j.physrep.2016.05.003.

[3] Barretta R, Brcic M, Canadija M, Luciano R, Marotti de Sciarra F. Application of gradient elasticity to armchair carbon nanotubes: size effects and constitutive parameters assessment. Eur J Mech Solid 2017;65:1–13. https://doi.org/10.1016/j.euromechsol.2017.03.002.

[4] Aifantis EC. Update on a class of gradient theories. Mech Mater 2003;35(3–6):259–80. https://doi.org/10.1016/S0167-6636(02)00278-8.

[5] Aifantis EC. On the gradient approach – relation to Eringen's nonlocal theory. Int J Eng Sci 2011;49(12):1367–77. https://doi.org/10.1016/j.ijengsci.2011.03.016.

[6] Polizzotto C. A gradient elasticity theory for second-grade materials and higher order inertia. Int J Solid Struct 2012;49(15–16):2121–37. https://doi.org/10.1016/j.ijsolstr.2012.04.019.

[7] Lim CW, Zhang G, Reddy JN. A higher-order nonlocal elasticity and strain gradient theory and its applications in wave propagation. J Mech Phys Solid 2015;78:298–313. https://doi.org/10.1016/j.jmps.2015.02.001.

[8] Apuzzo A, Barretta R, Canadija M, Feo L, Luciano R, Marotti de Sciarra F. A closed-form model for torsion of nanobeams with an enhanced nonlocal formulation. Composites Part B 2017;108:315–24. https://doi.org/10.1016/j.compositesb.2016.09.012.

[9] Bruno D, Greco F. Delamination in composite plates: influence of shear deformability on interfacial debonding. Cement Concr Compos 2001;23(1):33–45. https://doi.org/10.1016/S0958-9465(00)00068-8.

[10] Greco F, Lonetti P. Mixed mode dynamic delamination in fiber reinforced composites. Composites Part B 2009;40(5):379–92. https://doi.org/10.1016/j.compositesb.2009.03.003.

[11] Greco F, Luciano R. A theoretical and numerical stability analysis for composite micro-structures by using homogenization theory. Composites Part B 2011;42(3):382–401. https://doi.org/10.1016/j.compositesb.2010.12.006.

[12] Bruno D, Greco F, Lonetti P. A fracture-ALE formulation to predict dynamic debonding in FRP strengthened concrete beams. Composites Part B 2013;46:46–60. https://doi.org/10.1016/j.compositesb.2012.10.015.

[13] Greco F. A study of stability and bifurcation in micro-cracked periodic elastic composites including self-contact. Int J Solid Struct 2013;50(10):1646–63. https://doi.org/10.1016/j.ijsolstr.2013.01.036.

[14] Feo L, Greco F, Leonetti L, Luciano R. Mixed-mode fracture in lightweight aggregate concrete by using a moving mesh approach within a multiscale framework. Compos Struct 2015;123:88–97. https://doi.org/10.1016/j.compstruct.2014.12.037.

[15] Mindlin RD. Second gradient of strain and surface-tension in linear elasticity. Int J Solid Struct 1965;1(4):417–38. https://doi.org/10.1016/0020-7683(65)90006-5.

[16] Aifantis EC. On the role of gradients in the localization of deformation and fracture. Int J Eng Sci 1992;3(10):1279–99. https://doi.org/10.1016/0020-7225(92)90141-3.

[17] Polizzotto C. Gradient elasticity and nonstandard boundary conditions. Int J Solid Struct 2003;40(26):7399–423. https://doi.org/10.1016/j.ijsolstr.2003.06.001.

[18] Eringen A. On differential equations of nonlocal elasticity and solutions of screw dislocation and surface waves. J Appl Phys 1983;54(9):4703–10. https://doi.org/10.1063/1.332803.

[19] Eringen A. Nonlocal continuum field theories. New York: Springer; 2002.

[20] Romano G, Barretta R, Diaco M, Marotti de Sciarra F. Constitutive boundary conditions and paradoxes in nonlocal elastic nanobeams. Int J Mech Sci 2017;121:151–6. https://doi.org/10.1016/j.ijmecsci.2016.10.036.

[21] Romano G, Barretta R, Diaco M. On nonlocal integral models for elastic nano-beams. Int J Mech Sci 2017;131–132:490–9. https://doi.org/10.1016/j.ijmecsci.2017.07.013.

[22] Romano G, Luciano R, Barretta R, Diaco M. Nonlocal integral elasticity in nanostructures, mixtures, boundary effects and limit behaviours. Continuum Mech Therm 2018;30(3):641–55. https://doi.org/10.1007/s00161-018-0631-0.

[23] Romano G, Barretta R. Stress-driven versus strain-driven nonlocal integral model for elastic nano-beams. Composites Part B 2017;114:184–8. https://doi.org/10.1016/j.compositesb.2017.01.008.

[24] Romano G, Barretta R. Nonlocal elasticity in nanobeams: the stress-driven integral model. Int J Eng Sci 2017;115:14–27. https://doi.org/10.1016/j.ijengsci.2017.03.002.

[25] Barretta R, Čanadija M, Feo L, Luciano R, Marotti de Sciarra F, Penna R. Exact solutions of inflected functionally graded nano-beams in integral elasticity. Composites Part B 2018;142:273–86. https://doi.org/10.1016/j.compositesb.2017.12.022.

[26] Barretta R, Fabbrocino F, Luciano R, Marotti de Sciarra F. Closed-form solutions in stress-driven two-phase integral elasticity for bending of functionally graded nano-beams. Physica E 2018;97:13–30. https://doi.org/10.1016/j.physe.2017.09.026.

[27] Barretta R, Čanadija M, Luciano R, Marotti de Sciarra F. Stress-driven modeling of nonlocal thermoelastic behavior of nanobeams. Int J Eng Sci 2018;126:53–67. https://doi.org/10.1016/j.ijengsci.2018.02.012.

[28] Barretta R, Diaco M, Feo L, Luciano R, Marotti de Sciarra F, Penna R. Stress-driven integral elastic theory for torsion of nano-beams. Mech Res Commun 2018;87:35–41. https://doi.org/10.1016/j.mechrescom.2017.11.004.

[29] Barretta R, Faghidian SA, Luciano R, Medaglia CM, Penna R. Stress-driven two-phase integral elasticity for torsion of nano-beams. Composites Part B 2018;145:62–9. https://doi.org/10.1016/j.compositesb.2018.02.020.

[30] Apuzzo A, Barretta R, Luciano R, Marotti de Sciarra F, Penna R. Free vibrations of Bernoulli-Euler nano-beams by the stress-driven nonlocal integral model. Composites Part B 2017;123:105–11. https://doi.org/10.1016/j.compositesb.2017.03.057.

[31] Mahmoudpour E, Hosseini-Hashemi SH, Faghidian SA. Non-linear vibration analysis of FG nano-beams resting on elastic foundation in thermal environment using stress-driven nonlocal integral model. Appl Math Model 2018;57:302–15. https://doi.org/10.1016/j.apm.2018.01.021.

[32] Barretta R, Faghidian SA, Luciano R. Longitudinal vibrations of nano-rods by stress-driven integral elasticity. Mech Adv Mater Struct 2018. https://doi.org/10.1080/15376494.2018.1432806. in press.

[33] Dvorak GJ. Micromechanics of composite materials. New York: Springer; 2013.

[34] Barretta R, Feo L, Luciano R, Marotti de Sciarra F, Penna R. Functionally graded Timoshenko nanobeams: a novel nonlocal gradient formulation. Composites Part B 2016;100:208–19. https://doi.org/10.1016/j.compositesb.2016.05.052.

[35] Akgöz B, Civalek Ö. Free vibration analysis of axially functionally graded tapered Bernoulli–Euler microbeams based on the modified couple stress theory. Compos Struct 2013;98:314–22. https://doi.org/10.1016/j.compstruct.2012.11.020.

[36] Sedighi HM, Daneshmand F, Abadyan M. Dynamic instability analysis of electrostatic functionally graded doubly-clamped nano-actuators. Compos Struct 2015;124:55–64. https://doi.org/10.1016/j.compstruct.2015.01.004.

[37] Sedighi HM, Daneshmand F, Abadyan M. Modified model for instability analysis of symmetric FGM double-sided nano-bridge: corrections due to surface layer, finite conductivity and size effect. Compos Struct 2015;132:545–57. https://doi.org/10.1016/j.compstruct.2015.05.076.

[38] Sedighi HM, Keivani M, Abadyan M. Modified continuum model for stability analysis of asymmetric FGM double-sided NEMS: corrections due to finite conductivity, surface energy and nonlocal effect. Composites Part B 2015;83:117–33. https://doi.org/10.1016/j.compositesb.2015.08.029.

[39] Şimşek M. Nonlinear free vibration of a functionally graded nanobeam using nonlocal strain gradient theory and a novel Hamiltonian approach. Int J Eng Sci 2016;105:12–27. https://doi.org/10.1016/j.ijengsci.2016.04.013.

[40] Barretta R, Feo L, Luciano R, Marotti de Sciarra F. Application of an enhanced version of the Eringen differential model to nanotechnology. Composites Part B 2016;96:274–80. https://doi.org/10.1016/j.compositesb.2016.04.023.

[41] Togun N, Bağdatli S. Size dependent nonlinear vibration of the tensioned nanobeam based on the modified couple stress theory. Composites Part B 2016;97:255–62. https://doi.org/10.1016/j.compositesb.2016.04.074.

[42] Mercan K, Civalek Ö. Buckling analysis of Silicon carbide nanotubes (SiCNTs) with surface effect and nonlocal elasticity using the method of HDQ. Composites Part B 2017;114:34–45. https://doi.org/10.1016/j.compositesb.2017.01.067.

[43] Sedighi HM, Koochi A, Keivani M, Abadyan M. Microstructure-dependent dynamic behavior of torsional nano-varactor. Measure 2017;111:114–21. https://doi.org/10.1016/j.measurement.2017.07.011.

[44] Moory-Shirbani M, Sedighi HM, Ouakad HM, Najar F. Experimental and mathematical analysis of a piezoelectrically actuated multilayered imperfect microbeam subjected to applied electric potential. Compos Struct 2018;184:950–60. https://doi.org/10.1016/j.compstruct.2017.10.062.

[45] Faghidian SA. Integro-differential nonlocal theory of elasticity. Int J Eng Sci 2018;129:96–110. https://doi.org/10.1016/j.ijengsci.2018.04.007.

[46] Challamel N. Variational formulation of gradient or/and nonlocal higher-order shear elasticity beams. Compos Struct 2013;105:351–68. https://doi.org/10.1016/j.compstruct.2013.05.026.

[47] Marotti de Sciarra F, Barretta R. A gradient model for Timoshenko nanobeams. Physica E 2014;62:1–9. https://doi.org/10.1016/j.physe.2014.04.005.

[48] Ansari R, Faraji Oskouie M, Gholami R, Sadeghi F. Thermo-electro-mechanical vibration of postbuckled piezoelectric Timoshenko nanobeams based on the nonlocal elasticity theory. Composites Part B 2016;89:316–27. https://doi.org/10.1016/j.compositesb.2015.12.029.

[49] Bahrami A, Teimourian A. Study on the effect of small scale on the wave reflection in carbon nanotubes using nonlocal Timoshenko beam theory and wave propagation approach. Composites Part B 2017;91:492–504. https://doi.org/10.1016/j.compositesb.2016.02.004.

[50] Eltaher MA, Agwa M, Kabeel A. Vibration analysis of material size-dependent CNTs using energy equivalent model. J Appl Comput Mech 2018;4(2):75–86. https://doi.

The final version ofthis manuscript is available in COMPOSITES. PART B, ENGINEERING. DOI: 10.1016/j.compositesb.2018.07.036

org/10.22055/JACM.2017.22579.1136.
[51] Faghidian SA. On non-linear flexure of beams based on non-local elasticity theory. Int J Eng Sci 2018;124:49–63. https://doi.org/10.1016/j.ijengsci.2017.12.002.
[52] Akgöz B, Civalek Ö. Shear deformation beam models for functionally graded microbeams with new shear correction factors. Compos Struct 2014;112:214–25. https://doi.org/10.1016/j.compstruct.2014.02.022.
[53] Akgöz B, Civalek Ö. Effects of thermal and shear deformation on vibration response of functionally graded thick composite microbeams. Composites Part B 2017;129:77–87. https://doi.org/10.1016/j.compositesb.2017.07.024.
[54] Faghidian SA. Reissner stationary variational principle for nonlocal strain gradient theory of elasticity. Eur J Mech Solid 2018;70:115–26. https://doi.org/10.1016/j.euromechsol.2018.02.009.
[55] Wu CH. Cohesive elasticity and surface phenomena. Q Appl Math 1992;50(1):73–103. https://doi.org/10.1090/qam/1146625.
[56] Faghidian SA. Unified formulations of the shear coefficients in Timoshenko beam theory. J Eng Mech 2017;143(9). https://doi.org/10.1061/(ASCE)EM.1943-7889.0001297. 06017013–1:8.
[57] Barretta R. On the relative position of twist and shear centres in the orthotropic and fiberwise homogeneous Saint-Venant beam theory. Int J Solid Struct 2012;49(21):3038–46. https://doi.org/10.1016/j.ijsolstr.2012.06.003.
[58] Romano G, Barretta A, Barretta R. On torsion and shear of Saint-Venant beams. Eur J Mech Solid 2012;35:47–60. https://doi.org/10.1016/j.euromechsol.2012.01.007.
[59] Barretta R. Analogies between Kirchhoff plates and Saint-Venant beams under torsion. Acta Mech 2013;224(12):2955–64. https://doi.org/10.1007/s00707-013-0912-4.
[60] Barretta R. On Cesàro-Volterra method in orthotropic Saint-Venant beam. J Elasticity 2013;112(2):233–53. https://doi.org/10.1007/s10659-013-9432-7.
[61] Barretta R. Analogies between Kirchhoff plates and Saint-Venant beams under flexure. Acta Mech 2014;225(7):2075–83. https://doi.org/10.1007/s00707-013-1085-x.
[62] Faghidian SA. Unified formulation of the stress field of saint-Venant's flexure problem for symmetric cross-sections. Int J Mech Sci 2016;111–112:65–72. https://doi.org/10.1016/j.ijmecsci.2016.04.003.
[63] Romano G, Diaco M, Barretta R. Variational formulation of the first principle of continuum thermodynamics. Continuum Mech Therm 2010;22(3):177–87. https://doi.org/10.1007/s00161-009-0119-z.
[64] Gurtin ME, Fried E, Anand L. The mechanics and thermodynamics of continua. Cambridge: Cambridge University Press; 2010.
[65] Barretta R, Luciano R, Marotti de Sciarra F, Ruta G. Stress-driven nonlocal integral model for Timoshenko elastic nano-beams. Eur J Mech Solid 2018;72:275–86. https://doi.org/10.1016/j.euromechsol.2018.04.012.
[66] Reddy JN. Energy principles and variational methods in applied mechanics. third ed. New Jersey: Wiley; 2017.

The final version ofthis manuscript is available in COMPOSITES. PART B, ENGINEERING. DOI: 10.1016/j.compositesb.2018.07.036

FIGURES

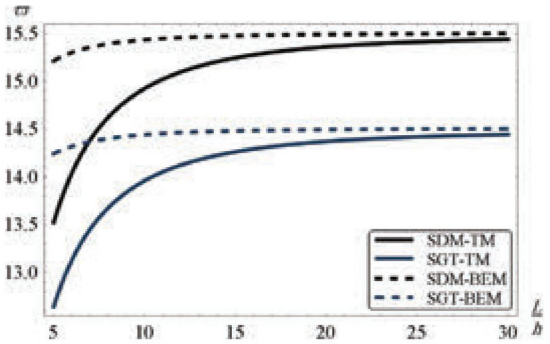

Fig. 7. Clamped-simply supported nano-beam: effects of the aspect ratio L/h on the dimensionless fundamental natural frequency ϖ for $\lambda = 0.1$, $E_2/E_1 = 1/4$, $n = 1$, $\rho_2/\rho_1 = 1/2$.

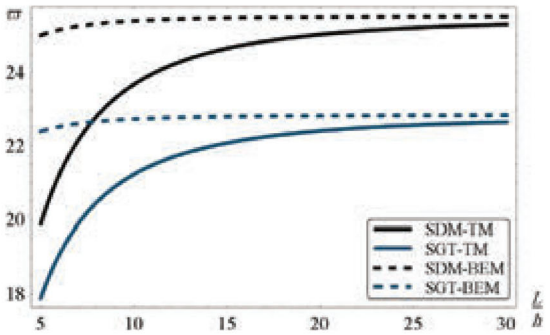

Fig. 8. Doubly clamped nano-beam: effects of the aspect ratio L/h on the dimensionless fundamental natural frequency ϖ for $\lambda = 0.1$, $E_2/E_1 = 1/4$, $n = 1$, $\rho_2/\rho_1 = 1/2$.

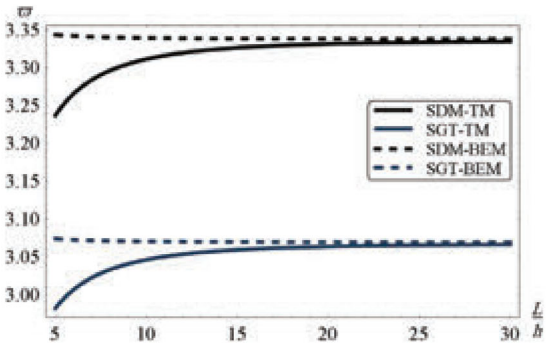

Fig. 9. Cantilever nano-beam: effects of the aspect ratio L/h on the dimensionless fundamental natural frequency ϖ for $\lambda = 0.1$, $E_2/E_1 = 1/4$, $n = 1$, $\rho_2/\rho_1 = 1/2$.

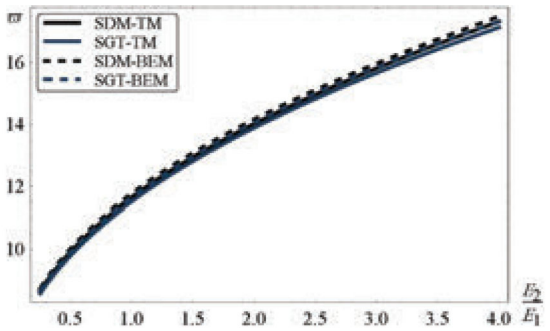

Fig. 10. Simply supported nano-beam: effects of the elastic modulus ratio E_2/E_1 on the fundamental natural frequency ϖ for $\lambda = 0.1$, $L/h = 10$, $n = 1$, $\rho_2/\rho_1 = 1/2$.

FIGURES

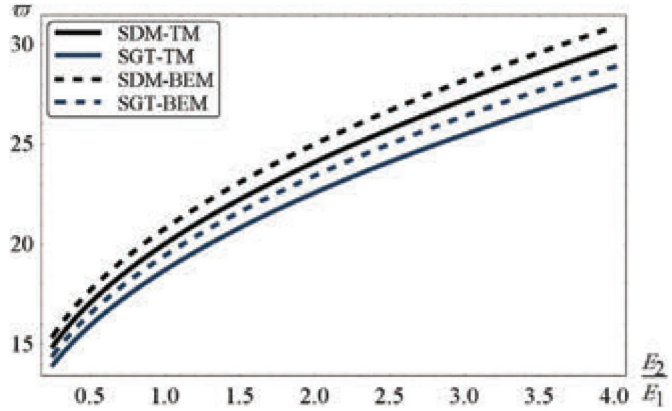

Fig. 11. Clamped-simply supported nano-beam: effects of the elastic modulus ratio E_2/E_1 on the fundamental natural frequency ϖ for $\lambda = 0.1$, $L/h = 10$, $n = 1$, $\rho_2/\rho_1 = 1/2$.

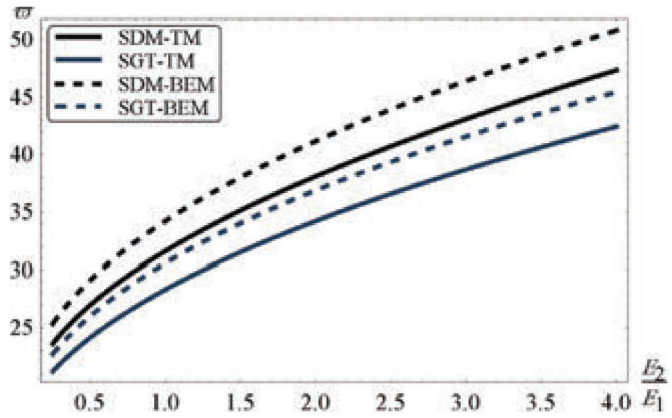

Fig. 12. Doubly clamped nano-beam: effects of the elastic modulus ratio E_2/E_1 on the fundamental natural frequency ϖ for $\lambda = 0.1$, $L/h = 10$, $n = 1$, $\rho_2/\rho_1 = 1/2$.

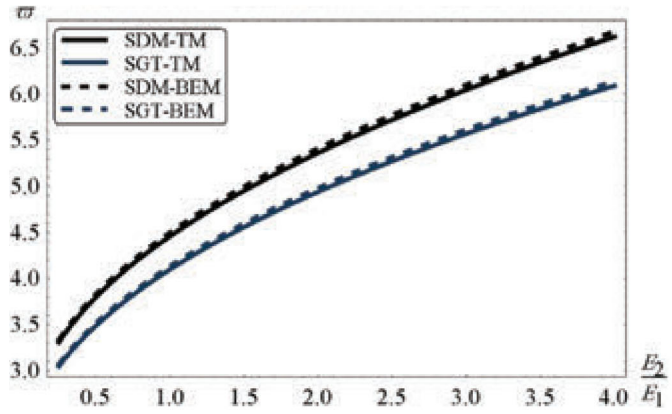

Fig. 13. Cantilever nano-beam: effects of the elastic modulus ratio E_2/E_1 on the fundamental natural frequency ϖ for $\lambda = 0.1$, $L/h = 10$, $n = 1$, $\rho_2/\rho_1 = 1/2$.

FIGURES

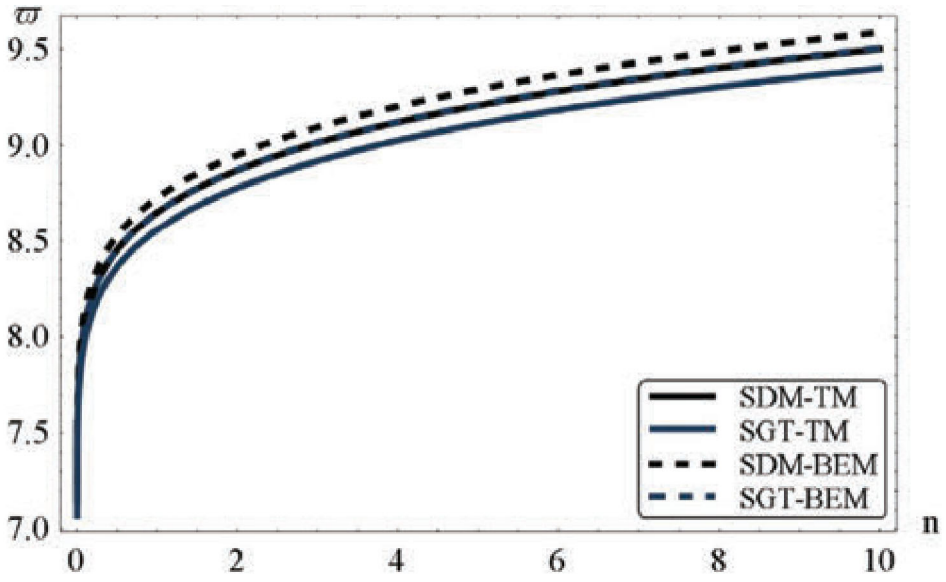

Fig. 14. Simply supported nano-beam: dimensionless fundamental natural frequency ϖ versus n for $\lambda = 0.1$, $L/h = 10$, $E_2/E_1 = 1/4$, $\rho_2/\rho_1 = 1/2$.

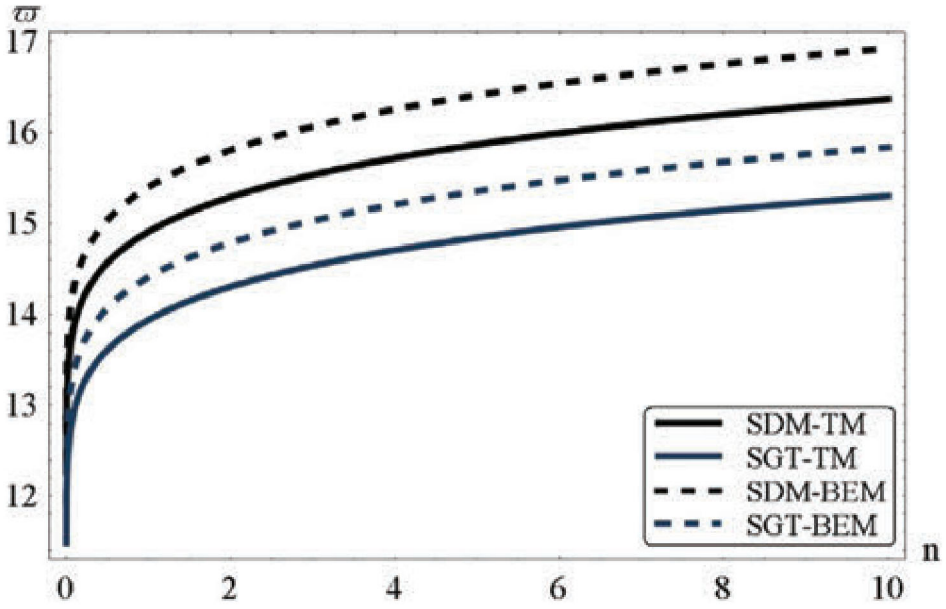

Fig. 15. Clamped-simply supported nano-beam: dimensionless fundamental natural frequency ϖ versus n for $\lambda = 0.1$, $L/h = 10$, $E_2/E_1 = 1/4$, $\rho_2/\rho_1 = 1/2$.

FIGURES

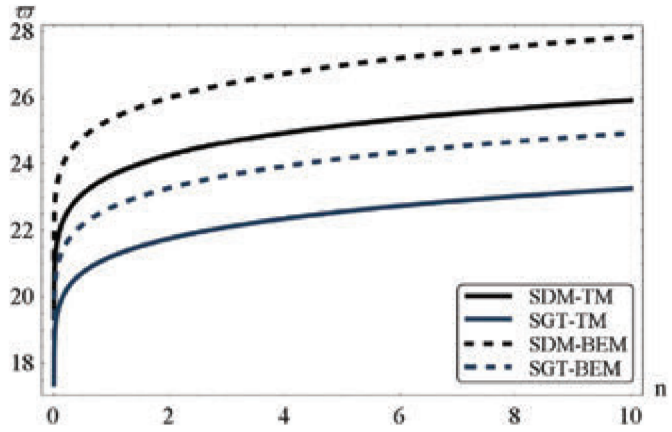

Fig. 16. Doubly clamped nano-beam: dimensionless fundamental natural frequency ϖ versus n for $\lambda = 0.1$, $L/h = 10$, $E_2/E_1 = 1/4$, $\rho_2/\rho_1 = 1/2$.

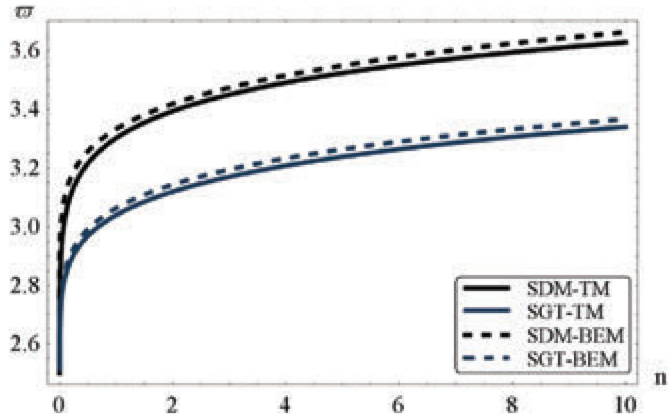

Fig. 17. Cantilever nano-beam: dimensionless fundamental natural frequency ϖ versus n for $\lambda = 0.1$, $L/h = 10$, $E_2/E_1 = 1/4$, $\rho_2/\rho_1 = 1/2$.

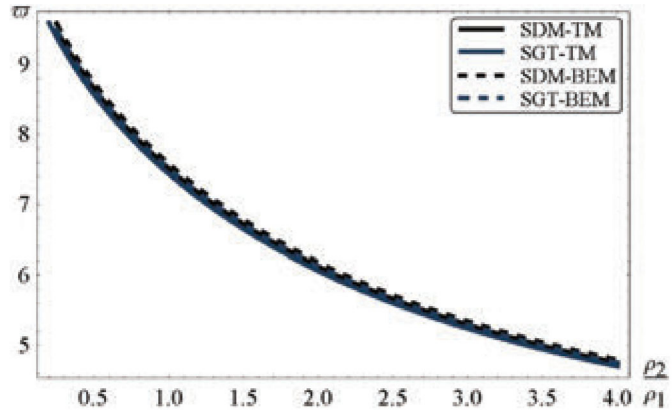

Fig. 18. Simply supported nano-beam: variations of the dimensionless fundamental natural frequency ϖ versus the material density ratio ρ_2/ρ_1 for $\lambda = 0.1$, $L/h = 10$, $E_2/E_1 = 1/4$, $n = 1$.

FIGURES

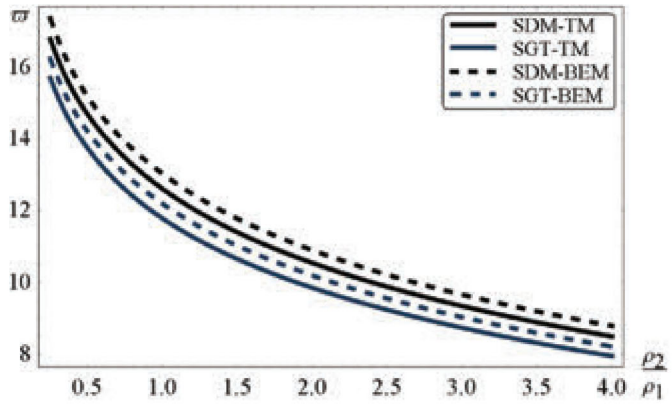

Fig. 19. Clamped-simply supported nano-beam: variations of the dimensionless fundamental natural frequency ϖ versus the material density ratio ρ_2/ρ_1 for $\lambda = 0.1$, $L/h = 10$, $E_2/E_1 = 1/4$, $n = 1$.

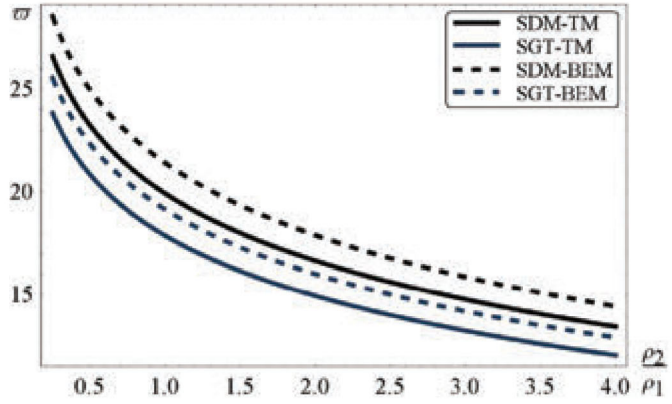

Fig. 20. Doubly clamped nano-beam: variations of the dimensionless fundamental natural frequency ϖ versus the material density ratio ρ_2/ρ_1 for $\lambda = 0.1$, $L/h = 10$, $E_2/E_1 = 1/4$, $n = 1$.

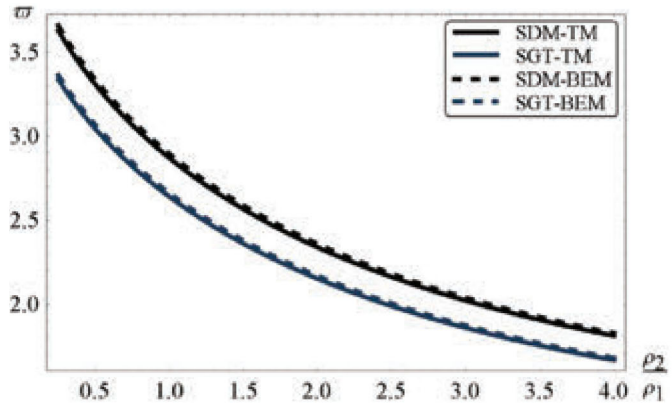

Fig. 21. Cantilever nano-beam: variations of the dimensionless fundamental natural frequency ϖ versus the material density ratio ρ_2/ρ_1 for $\lambda = 0.1$, $L/h = 10$, $E_2/E_1 = 1/4$, $n = 1$.

FIGURES

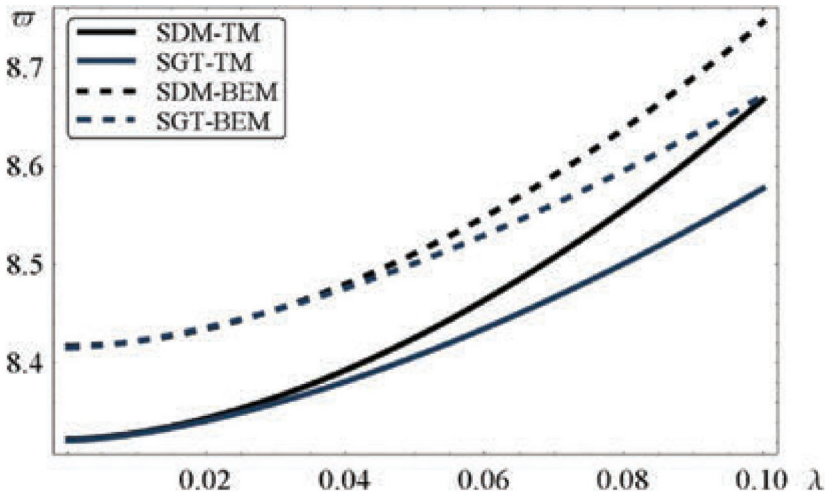

Fig. 22. Simply supported nano-beam: dimensionless fundamental natural frequency ϖ versus the characteristic parameter λ for $L/h = 10$, $E_2/E_1 = 1/4$, $n = 1$, $\rho_2/\rho_1 = 1/2$.

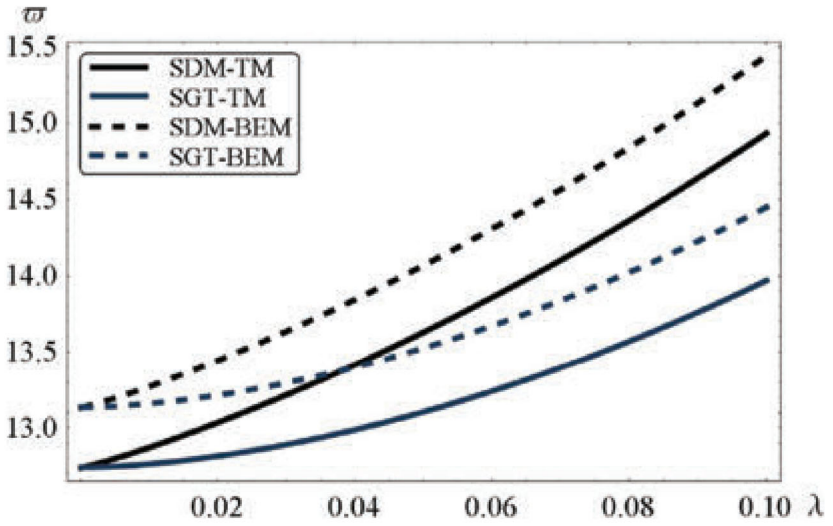

Fig. 23. Clamped-simply supported nano-beam: dimensionless fundamental natural frequency ϖ versus the characteristic parameter λ for $L/h = 10$, $E_2/E_1 = 1/4$, $n = 1$, $\rho_2/\rho_1 = 1/2$.

FIGURES

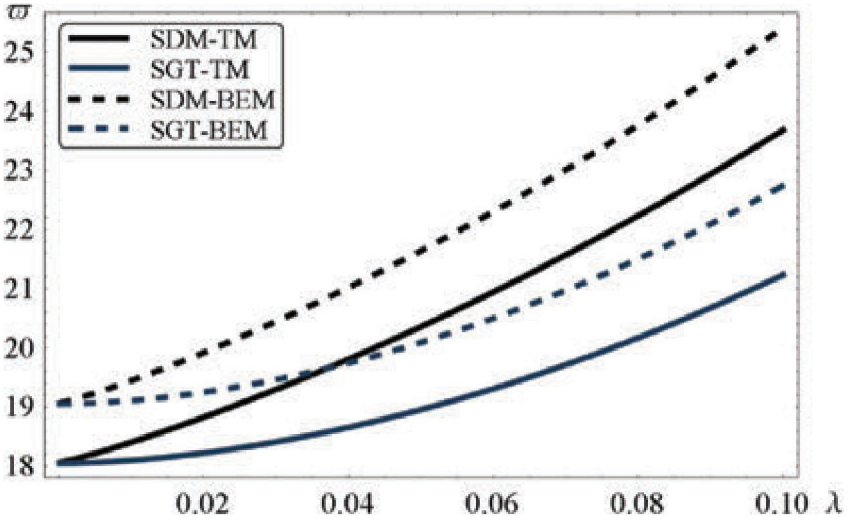

Fig. 24. Doubly clamped nano-beam: dimensionless fundamental natural frequency ϖ versus the characteristic parameter λ for $L/h = 10$, $E_2/E_1 = 1/4$, $n = 1$, $\rho_2/\rho_1 = 1/2$.

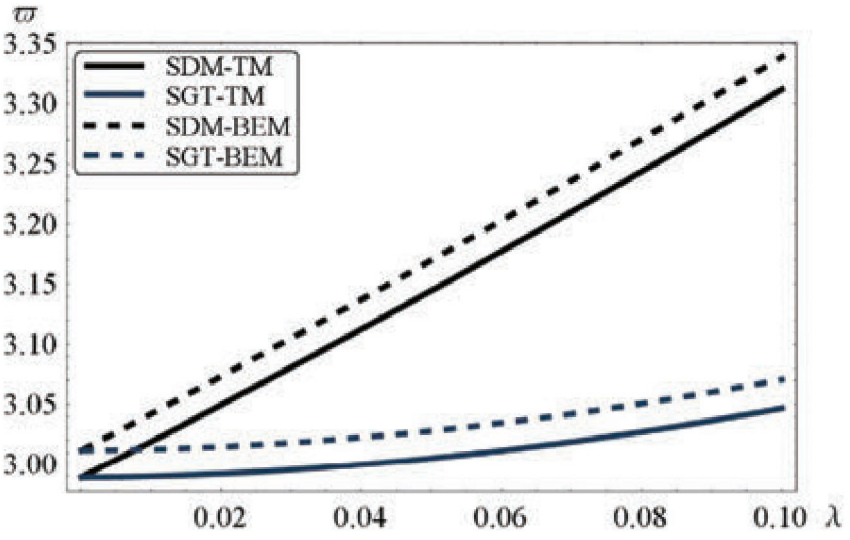

Fig. 25. Cantilever nano-beam: dimensionless fundamental natural frequency ϖ versus the characteristic parameter λ for $L/h = 10$, $E_2/E_1 = 1/4$, $n = 1$, $\rho_2/\rho_1 = 1/2$.

FIGURES

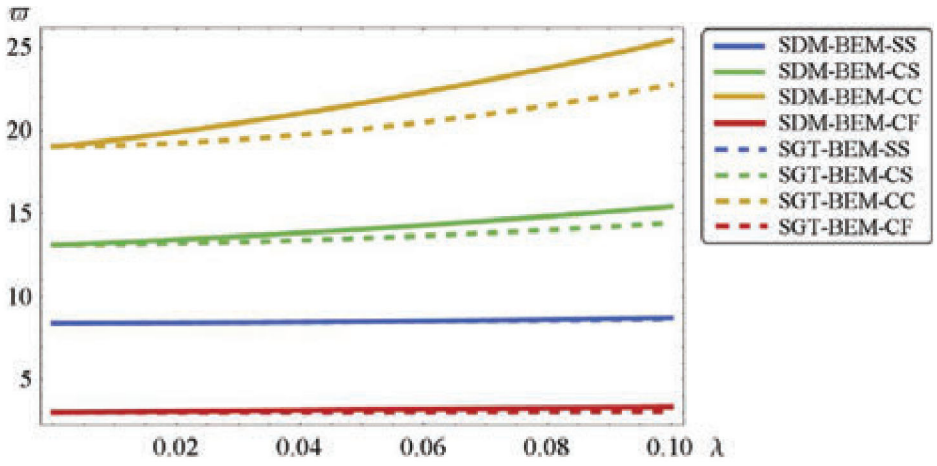

Fig. 26. Bernoulli-Euler nano-beam: effects of the boundary conditions on the dimensionless fundamental natural frequency ϖ versus the characteristic parameter λ.

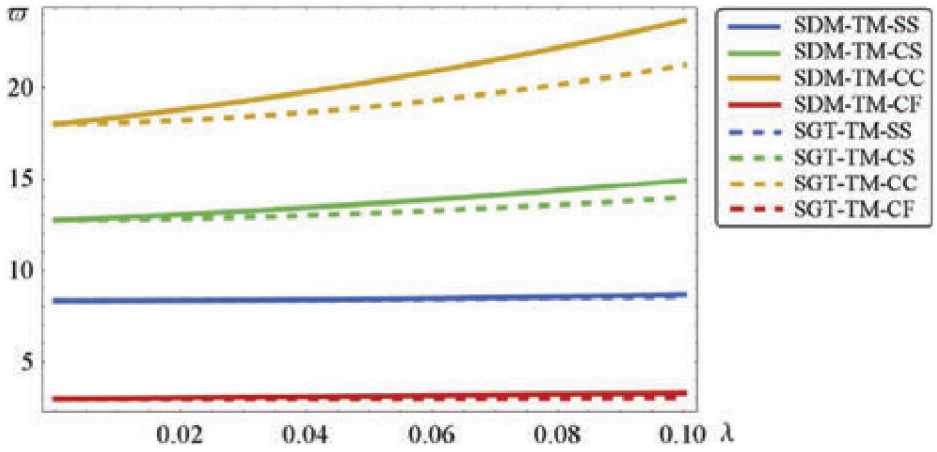

Fig. 27. Timoshenko nano-beam: effects of the boundary conditions on the dimensionless fundamental natural frequency ϖ versus the characteristic parameter λ.

FIGURES

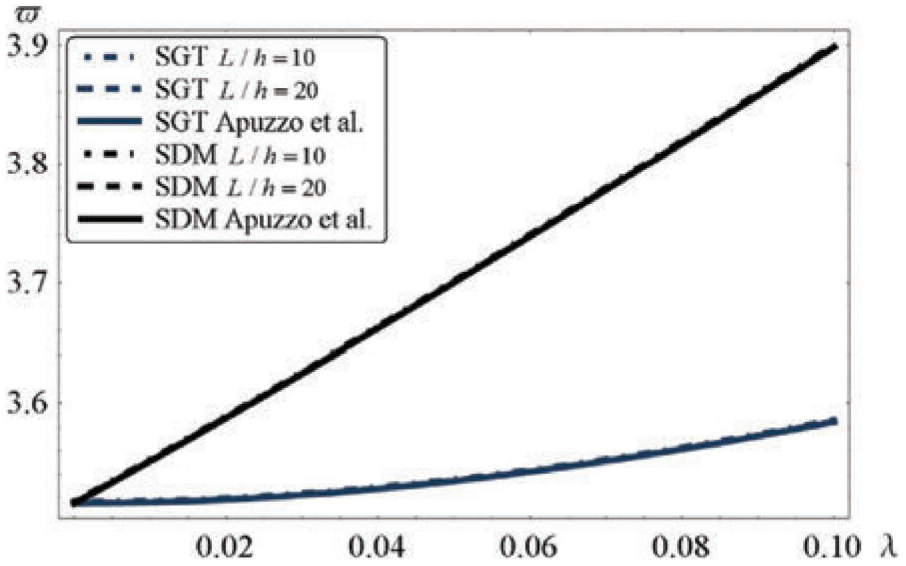

Fig. 5. Cantilever Bernoulli-Euler nano-beam: dimensionless fundamental natural frequency ϖ versus the characteristic parameter λ for different aspect ratio L/h.

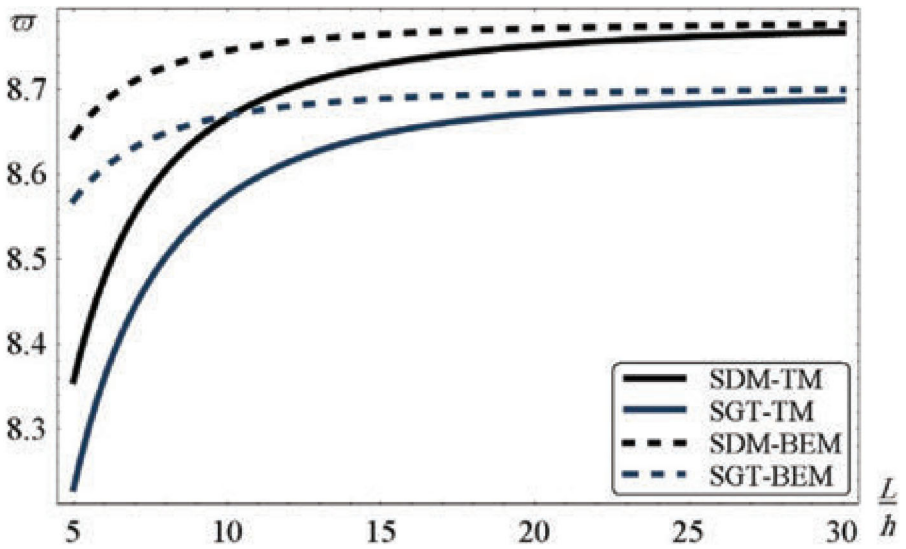

Fig. 6. Simply supported nano-beam: effects of the aspect ratio L/h on the dimensionless fundamental natural frequency ϖ for $\lambda = 0.1$, $E_2/E_1 = 1/4$, $n = 1$, $\rho_2/\rho_1 = 1/2$.

FIGURES

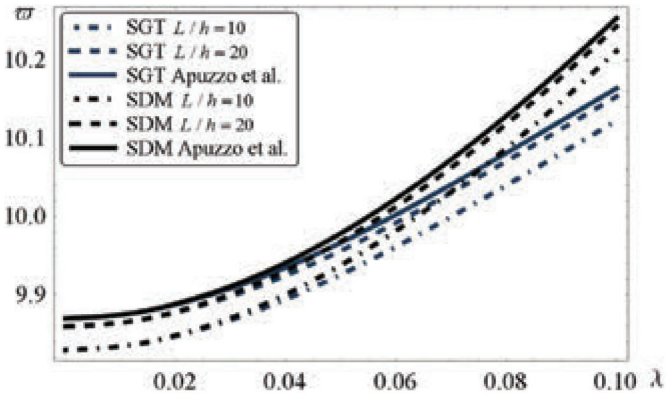

Fig. 2. Simply-supported Bernoulli-Euler nano-beam: dimensionless fundamental natural frequency ϖ versus the characteristic parameter λ for different aspect ratio L/h.

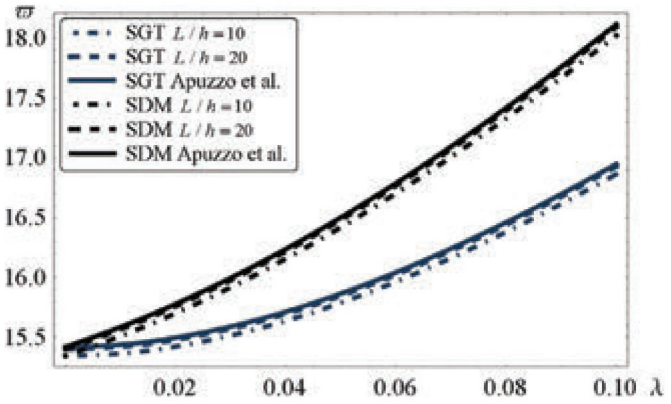

Fig. 3. Clamped-simply supported Bernoulli-Euler nano-beam: dimensionless fundamental natural frequency ϖ versus the characteristic parameter λ for different aspect ratio L/h.

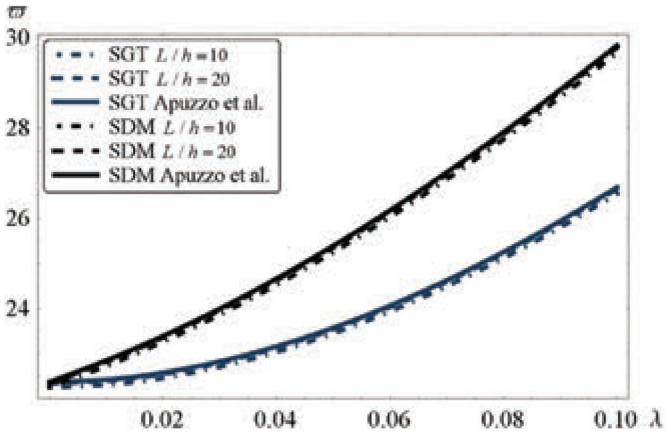

Fig. 4. Doubly-clamped Bernoulli-Euler nano-beam: dimensionless fundamental natural frequency ϖ versus the characteristic parameter λ for different aspect ratio L/h.

FIGURES

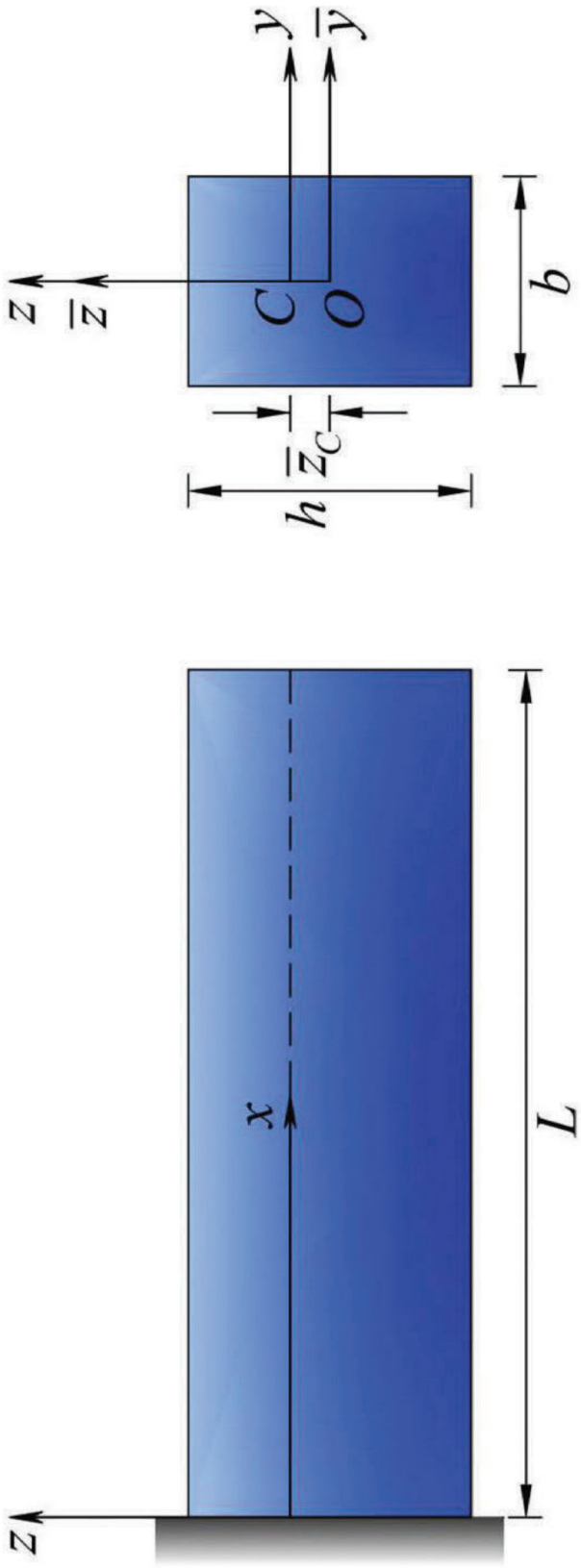

Fig. 1. Coordinate system and configuration of FG Timoshenko nano-beam.